Effects of parametric disorder on a stationary bifurcation

M. Hammele, S. Schuler, W. Zimmermann

Theoretical Physics, University of Saarland, D-66041 Saarbrücken, Germany

Abstract

Effects of a frozen random contribution to the control parameter are investigated in terms of the complex Ginzburg–Landau equation for a stationary bifurcation. The threshold of the bifurcation from the homogeneous basic state is reduced by a random contribution even with a vanishing spatial mean value, as shown by three different approaches, by a perturbation calculation, by a self-consistent iteration method and by a fully numerical solution of the linear part of the Ginzburg-Landau equation. For an arbitrary noise strength the nonlinear stationary solutions are numerically determined for a set of selected parameters. In the limit of weak random contributions analytical expressions are derived in terms of two different perturbation expansions, which describe already several trends of the random effects beyond threshold. The spatial modulation of the solutions, for instance, increases with the noise amplitude, but decreases with increasing distance from threshold.

Key words: pattern formation, pattern selection, Hydrodynamic stability
PACS: 47.54.+r, 47.20.Ky

1 Introduction

Pattern formation is investigated particularly in spatially uniform systems [1,2], in order to understand at first the essence of the underlying basic mechanisms. However, real systems are not always perfectly uniform and include heterogeneities, which may become nonnegligible with increasing experimental resolution. Heterogeneities may modify a bifurcation scenario, such as shifting the threshold and the nonlinear behavior beyond a bifurcation. It is therefore an interesting problem, what are such changes, how robust are the generic pattern formation processes with respect to small inhomogeneities and above

Email address: wz@lusi.uni-sb.de (W. Zimmermann).

which strength do the inhomogeneities change the bifurcation behavior qualitatively? Here we focus on the effects of heterogeneities on a stationary bifurcation, where the spatially varying parameters occur multiplicatively in the respective model equations.

Rayleigh–Bénard convection [3,4] and Taylor–Vortex flow [3,5] are two systems, where the effects of inhomogeneities have already been investigated rather early. In both systems the effects of ramps, of periodic modulations or of statistical distributed heterogeneities on different aspects of pattern formation, such as wavelength selection etc. have been studied [6–25]. In several of these examples the spatial variation of the parameters was restricted to one direction [6–17] and in others either the modulation depends on two spatial variables or the effects of a one–dimensional modulation on a two-dimensional pattern was investigated [18–25]. Recently, a number of investigations about heterogeneity effects were also focusing on the Turing instability in chemical reactions [26–30], on excitable media [31–34], or on optical systems [35].

Here, we investigate the influence of a time–independent either spatially periodic or spatially varying random contribution to the control parameter on a supercritical bifurcation from a homogeneous basic state to a spatially periodic state. Close to the threshold of such a supercritical bifurcation with wave number q_c, a real field $u(x,t)$ may be written as a product of the fast varying function $\propto e^{iq_c x}$ and the amplitude $A(x,t)$

$$u(x,t) = A(x,t)e^{iq_c x} + A^*(x,t)e^{-iq_c x} \ . \tag{1}$$

There are many systems showing a transition to a one–dimensional periodic state of this type, as for instance the famous Rayleigh–Bénard convection, the Taylor vortex flow, electroconvection [36] or the Turing instability. Here we will focus on values of the control parameter close to the threshold, where only long–wavelength modulations of the spatially periodic function $\propto \exp(iq_c x)$ are relevant. Such variations are commonly described by a slowly varying amplitude $A(x,t)$ of the periodic pattern given in Eq. (1) for which the well-known Ginzburg-Landau equation [37,38]

$$\tau_0 \partial_t A = \varepsilon A + \xi_0^2 \partial_x^2 A - g \mid A \mid^2 A \tag{2}$$

may be derived. Here τ_0 is the relaxation time, ε measures the distance from threshold of the spatially periodic pattern, ξ_0 is the coherence length and the nonlinear coefficient g determines the amplitude of the pattern as a function of the control parameter ε, as for instance with $A \propto \sqrt{\varepsilon/g}$ and $g > 0$ close to a supercritical (forward) bifurcation. This amplitude equation is one of the simplest models describing a bifurcation from an initial state $A = 0$ to a stationary and spatially varying pattern $A \neq 0$. A spatial modulation of the control parameter $\varepsilon \to \varepsilon + M(x)$, which describes for instance major effects of a rough container boundary in Rayleigh-Bénard convection as estimated

in Ref. [12], leads to a modification of the bifurcation as shown in this work. It leads for instance to a shift of the threshold but leaves the bifurcation still perfect, whereas an additive contribution $f(x,t)$ in Eq. (2) makes the bifurcation imperfect.

In section 2 we describe the model and three different types of modulations of the control parameter. The effects of these modulations on the threshold are calculated in section 3 by solving the linear part of Eq. (3) by three different methods, whereby their strengths and the deficiencies are compared with each other. In section 3.1 a perturbation method is employed, in section 3.2 a full numerical solution in Fourier-space is given and in section 3.3 a self-consistent approach is introduced. Beyond the threshold the dependence of the nonlinear solution on the distance from the threshold is also changed by the modulation of the control parameter as described in section 4. In section 4.1 the nonlinear equation is solved numerically for a typical set of parameters and in section 4.2 the nonlinear solutions are determined in the range of small modulation amplitudes by the Poincaré-Lindstedt expansion. The results of this expansion are compared with the results obtained by solving the nonlinear equation numerically. A modified expansion of the nonlinear solution far beyond threshold is described in section 4.3 and the work ends with the discussion of the results and concluding remarks in section 5.

2 Model equation

The effects of a time-independent random contribution $M(x)$ to the control parameter are investigated near a bifurcation–point or phase transition in terms of the complex Ginzburg–Landau equation with real coefficients

$$\tau_0 \partial_t A = \left[\varepsilon + M(x) + \xi_0^2 \partial_x^2\right] A - g \mid A \mid^2 A \; . \tag{3}$$

$M(x)$ is assumed to be either spatially periodic or a random function, as specified in the following subsection.

2.1 Three types of spatial modulations $M(x)$

Spatially periodic modulations of the control parameter have already some tradition [6–15] and some trends to be expected for a random function $M(x)$ in Eq. (3) can already be investigated in terms of a periodic function

$$M(x) = 2G \cos(kx) \; . \tag{4}$$

For a randomly varying modulation $M(x) = \xi(x)$, we assume a vanishing mean value and a δ-correlated second moment [39]:

$$\langle\, \xi(x) \,\rangle = 0 \;, \tag{5a}$$

$$\langle\, \xi(x)\; \xi(x') \,\rangle = D\, \delta(x - x') \,. \tag{5b}$$

The amplitude D in Eq. (5b) is a measure for the noise intensity and the δ-correlation expresses, that the random function $M(x)$ is statistically independent at each location $x \neq x^{'}$. The Fourier transform of the correlation function (5b) is also δ-correlated $\langle \xi^*(q)\xi(q')\rangle = 2\pi D\delta(q - q')$ and otherwise independent of the wave number.

In a third example we assume an Ornstein-Uhlenbeck process $M(x) = \omega(x)$ in space, where $\omega(x)$ is generated by a white noise $\xi(x)$ via the first order differential equation [39,40]

$$\frac{\partial \omega(x)}{\partial x} = -\frac{\omega(x)}{\ell} + \frac{\xi(x)}{\ell} \tag{6}$$

for different values of the correlation length ℓ. $\omega(x)$ is a so-called colored noise with vanishing mean value, where $\omega(x)$ and $\omega(x')$ are correlated at different sites $x \neq x'$ with an exponential decay of the correlation on a typical length ℓ as follows:

$$\langle\, \omega(x) \,\rangle = 0 \;, \tag{7a}$$

$$\langle\, \omega(x)\; \omega(x') \,\rangle = \frac{D}{2\,\ell}\, e^{-|x-x'|/\ell} \;. \tag{7b}$$

The exponential decay in Eq. (7b) leads to a wave number dependence of its Fourier transformation

$$< \omega^*(q)\; \omega(q') >= \frac{2\pi D\delta(q - q^{'})}{1 + \ell^2 q^2} \,. \tag{8}$$

The correlation function of white noise is recovered from Eq. (7b) and Eq. (8) in the limit $\ell \to 0$ by keeping D fixed.

Numerically the model in Eq. (3) may be solved on a finite grid with grid spacing $\Delta x = L/N$, the number N of grid points, and the position $x_j = j\Delta x$ of the sites. An alternative approach is a solution in terms of N Fourier modes, as presented in Sec. 2.2. On a discrete lattice the autocorrelation function of the random process $\xi(x)$ takes the form

$$\langle\, \xi(x_i)\xi(x_j) \,\rangle = \frac{D}{\Delta x}\delta_{i,j} \;, \tag{9}$$

where the random process [41]

$$\xi_j = \sqrt{\frac{12D}{\Delta x}} \left(\zeta_j - \frac{1}{2} \right) \tag{10}$$

is expressed in terms of uniformly distributed random numbers $0 \leq \zeta_j \leq 1$ that are generated by a standard pseudo–random number generator with $\langle \zeta_j \rangle = 1/2$ and $\langle \zeta_j^2 \rangle = 1/12$. Uniformly distributed random numbers ζ_j are used because the rare but huge fluctuations of a Gaussian distributed random process are unrealistic for modeling, for instance, the roughness of the two opposite container boundaries in Rayleigh-Bénard convection [3,4], or the roughness of the two cylinders of a Taylor-Couette system [3,5,16].

2.2 Solution scheme of Eq. (3) in Fourier-space

The long-wavelength contributions to $M(x)$ cover the major effects of the modulation because the short-wavelength contributions are to a large extend smoothed out by the diffusion term in Eq. (3) (see e.g. Fig. 2). Therefore, the analysis can often be simplified by focusing especially in long systems on the long-wavelength portions of the solution of Eq. (3), in order to reduce the computational effort considerably. For this purpose the real function $M(x)$ may be represented in a finite system of length L in terms of a Fourier series

$$M(x) = \sum_{n=-N}^{N} c_n e^{inkx} , \qquad \text{with} \quad c_{-n} = c_n^* , \ \text{and} \ \ c_0 = 0 , \tag{11}$$

where the Fourier-coefficients c_n and the wave number k are given by

$$c_n = \frac{1}{L} \int_0^L dx \, M(x) e^{-inkx} \qquad \text{and} \qquad k = \frac{2\pi}{L} . \tag{12}$$

We have assumed for reasons of simplicity, that the constant contribution c_0 to $M(x)$ is already included in the non–varying part of the control parameter ε. Inherent of this ansatz is the assumption of periodic boundary conditions for Eq. (3). However, this assumption is actually a rather weak one, especially in long systems and when we are interested in mean values as for instance in the mean shift of the threshold for an ensemble of random functions $\xi(x)$ or $\omega(x)$.

A representation of the solution of Eq. (3) in terms of a Fourier-series

$$A(x) = \sum_{n=-N}^{N} F_n e^{inkx} \ , \tag{13}$$

together with a successive projection $\int dx \exp(-ijkx) \ldots$ of the linear part of Eq. (3) leads to the following linear eigenvalue problem

$$\left(\varepsilon - \xi_0^2 (jk)^2\right) F_j + \sum_{l=-N}^{N} c_{j-l} F_l = 0 \qquad (j = -N \ldots N) \,, \tag{14}$$

where the smallest eigenvalue gives the threshold ε_c. The amplitudes c_n of the Fourier expansion of $M(x)$ provide a coupling between the modes F_l of the linear solution $A(x)$ and give rise to a threshold shift. This eigenvalue problem will be analyzed in the next section by a perturbation method, a fully numerical calculation as well as by a self-consistent iteration method. Including the nonlinear term of Eq. (3), the nonlinear solutions of this equation are obtained by using a standard pseudo-spectral code.

3 Determination of the threshold

The effects of a control parameter modulation $M(x)$ on the threshold of a stationary bifurcation are calculated by three different methods in this section. In the absence of modulations the linear part of Eq. (2) has constant coefficients and it is solved by the ansatz $A(x,t) = F \exp(iqx + \lambda t)$. The threshold for the instability of the solution $A = 0$ is defined by a vanishing growth rate, $\lambda = 0$. This neutral stability condition provides an expression for the control parameter $\varepsilon(q)$ as a function of the wave number q, the so-called *neutral curve*, which has for the Ginzburg–Landau model in Eq. (2) a parabolic shape

$$\varepsilon_0(q) = \xi_0^2 q^2 \,. \qquad \text{(neutral curve)} \tag{15}$$

This expression takes its minimum at $q = 0$ with the critical value $\varepsilon_c = \varepsilon_0(q = 0) = 0$ at this point. Taking into account the modulation $M(x)$, Eq. (3) describes a parametrically driven system. For this case the threshold is always negative $\varepsilon_c < 0$ and therefore lower than for the unmodulated system, as we will show in this section. The actual values of ε_c depend on the amplitudes of $M(x)$ as well as on its spatial form.

For small modulation amplitudes of $M(x)$ the threshold shift is calculated by a perturbation method as described in Sec. 3.1. For arbitrary modulation amplitudes and an arbitrary length L of the system, the threshold is calculated numerically by solving the eigenvalue problem in Eq. (14) for a selected set

of parameters in Sec. 3.2 as well as by a self–consistent iteration scheme in Sec. 3.3. The results obtained by these three different approaches are compared with each other.

3.1 Perturbation method for small amplitudes of $M(x)$

We introduce a small parameter $\eta \ll 1$ in order to express $M(x) = \eta \bar{M}(x)$ and $c_n = \eta \bar{c}_n$ for small modulation amplitudes in terms of a function $\bar{M}(x) \propto O(1)$ and of amplitudes $\bar{c}_n \propto O(1)$ of the order unity. In this limiting case, the effects of the modulation on the solution $A(x)$ and on the threshold ε_c may be calculated up to leading orders by a perturbation expansion for the control parameter ε, the solution $A(x)$, and the Fourier amplitudes F_j:

$$\varepsilon_c = \varepsilon_c^{(0)} + \eta \varepsilon_c^{(1)} + \eta^2 \varepsilon_c^{(2)} + \dots \,, \tag{16a}$$

$$A_c(x) = A_c^{(0)}(x) + \eta A_c^{(1)}(x) + \eta^2 A_c^{(2)}(x) + \dots \,, \tag{16b}$$

$$F_j = F_j^{(0)} + \eta F_j^{(1)} + \eta^2 F_j^{(2)} + \dots \,. \tag{16c}$$

Using these expansions, the linear part of Eq. (3) can be sorted with respect to powers of the small parameter η

$$\eta^0 : \;\; \mathcal{L}_0 A_c^{(0)} = 0 \,, \tag{17a}$$

$$\eta^1 : \;\; \mathcal{L}_0 A_c^{(1)} = -[\bar{M}(x) + \varepsilon_c^{(1)}] A_c^{(0)} \,, \tag{17b}$$

$$\eta^2 : \;\; \mathcal{L}_0 A_c^{(2)} = -[\bar{M}(x) + \varepsilon_c^{(1)}] A_c^{(1)} - \varepsilon_c^{(2)} A_c^{(0)} \,, \tag{17c}$$

$$\dots$$

where the linear operator $\mathcal{L}_0$ is given by

$$\mathcal{L}_0 = \varepsilon_c^{(0)} + \xi_0^2 \partial_x^2 \,. \tag{18}$$

A successive solution of this hierarchy gives the leading order corrections $\varepsilon_c^{(j)}$ and $A_c^{(j)}(x)$ of the solution of the linear part of Eq. (3). Representing also $A_c^{(j)}(x)$ by a Fourier series

$$A_c^{(j)}(x) = \sum_{n=-\infty}^{\infty} F_n^{(j)} e^{inkx} \quad \text{with} \quad F_n^{(j)} = \frac{1}{L} \int_0^L dx \, A_c^{(j)}(x) e^{-inkx} \,, \tag{19}$$

then this hierarchy of equations takes the following form:

$$\eta^0: \quad \widetilde{\mathcal{L}}_{0n} F_n^{(0)} = 0\,, \tag{20a}$$

$$\eta^1: \quad \widetilde{\mathcal{L}}_{0n} F_n^{(1)} = -\sum_{l=-\infty}^{\infty} \bar{c}_{n-l} F_l^{(0)} - \varepsilon_c^{(1)} F_n^{(0)}\,, \tag{20b}$$

$$\eta^2: \quad \widetilde{\mathcal{L}}_{0n} F_n^{(2)} = -\sum_{l=-\infty}^{\infty} \bar{c}_{n-l} F_l^{(1)} - \varepsilon_c^{(1)} F_n^{(1)} - \varepsilon_c^{(2)} F_n^{(0)}\,, \tag{20c}$$

$$\ldots$$

with the transformed linear operator $\widetilde{\mathcal{L}}_{0n} = \varepsilon_c^{(0)} - \xi_0^2 (nk)^2$.

Equation (20a) corresponds to the unperturbed linear equation and its spatially homogeneous solution $F_n^{(0)} = F_0 \delta_{0,n}$ with a real amplitude F_0 provides the lowest threshold at $\varepsilon_c^{(0)} = 0$, as already mentioned above. Accordingly, one has for $n = 0$ in Eq. (20b) $\widetilde{\mathcal{L}}_{00} = 0 = \widetilde{\mathcal{L}}_{00} F_0^{(1)}$, and since $M(x)$ does not include a spatially independent contribution, i.e. $c_0 = 0$, one obtains $\varepsilon_c^{(1)} = 0$. For $n \neq 0$ the inhomogeneous Eq. (20b) yields

$$F_n^{(1)} = \frac{F_0 \bar{c}_n}{\xi_0^2 (nk)^2} \tag{21}$$

and with Eq. (19), $A_c^{(1)}(x)$ may be expressed by the series

$$A_c^{(1)}(x) = {\sum_{n=-\infty}^{\infty}}' \frac{F_0 \bar{c}_n}{\xi_0^2 (nk)^2}\, e^{inkx}\,, \tag{22}$$

where the prime indicates a summation excluding $n = 0$.

According to $\widetilde{\mathcal{L}}_{00} = 0 = \widetilde{\mathcal{L}}_{00} F_0^{(2)}$ the right hand side in Eq. (20c) must vanish for $n = 0$, which provides an expression for the leading order threshold shift

$$\varepsilon_c^{(2)} = -2 \sum_{n=1}^{\infty} \frac{|\bar{c}_n|^2}{\xi_0^2 (nk)^2}\,. \tag{23}$$

For a *harmonic modulation* $M(x) = 2G \cos(Qx)$ with the amplitude $G = \eta \bar{G}$ and wave number $Q = jk$, one has $\bar{c}_n = \bar{G}(\delta_{n,j} + \delta_{n,-j})$ and according to Eq. (23) the threshold shift is

$$\varepsilon_c^{(2)} = -\frac{2\bar{G}^2}{\xi_0^2 Q^2}\,. \qquad \text{(threshold harmonic modulation)} \tag{24}$$

In the very special case, where all Fourier-coefficients coincide, $|\bar{c}_n| = \bar{G}$, the sum in Eq. (23) can be evaluated and one obtains

$$\varepsilon_c^{(2)} = -\frac{2\bar{G}^2}{\xi_0^2 k^2} \zeta(2) = -\frac{2\bar{G}^2}{\xi_0^2 k^2} \frac{\pi^2}{6}\,, \tag{25}$$

with the Riemann Zeta-function $\zeta(z)$. A comparison between the results given by Eq. (24) and Eq. (25) emphasizes that the major contributions to the threshold shift are due to the long-wavelength modulation with $Q = k$, because all the higher harmonics contribute to the threshold shift only 65% of that of the first mode. The dependence of the threshold shift on the coherence length ξ_0 is unchanged by including higher harmonics. This result indicates that also in the case of a random function $M(x)$ the contributions of short-wavelengths will be small.

However, within the presented perturbation scheme the threshold diverges with the system length as $\varepsilon_c^{(2)} \propto -L^2$, i.e. for a small wave number $k = 2\pi/L$. In this limit, $k \leq \eta$, the first order contribution $\eta A_c^{(1)} \propto \eta \bar{G}/k^2$ becomes of the order of "1" or larger. The correction $\eta A_c^{(1)}$ is therefore not small anymore compared to the unperturbed solution $A_c^{(0)}$ and the assumption made for the perturbation calculation is violated.

Another quantity for the characterization of the effects of the modulation is the mean wave number

$$q_m = \frac{\sum_n nk|F_n|^2}{\sum_n |F_n|^2} \tag{26}$$

that takes with the expression for the Fourier amplitudes, given in Eq. (21) at leading order in η the following form

$$q_m = \eta^2 \sum_{n=1}^{\infty} \frac{2\,|\bar{c}_n|^2}{\xi_0^4 (nk)^3} + O(\eta^4)\ . \tag{27}$$

For a harmonic modulation, as discussed above, one obtains for the mean wave number

$$q_m = \frac{2G^2}{\xi_0^4 Q^3} + O(\eta^4) \qquad (Q = jk)\ . \tag{28}$$

3.1.1 Modified neutral curve

Up to this point, Eqs. (17) have only been solved for constant solutions $A_0 = const.$ of the lowest order Eq. (17a). However, the latter one also has periodic solutions $\propto \exp(iqx)$ that grow above the neutral curve given by Eq. (15). It is an interesting question, how the threshold of these periodic solutions along the neutral curve $\varepsilon_0(q)$ is changed by a modulation $M(x)$. For a periodic modulation with wave number k, one obtains in the range $q < k/2$ and up to leading order in G the modified neutral curve as given by

$$\varepsilon_0(q) = \xi_0^2 q^2 - \eta^2 \frac{2\bar{G}^2}{\xi_0^2} \frac{1}{k^2 - (2q)^2} + \cdots . \tag{29}$$

The corrections to the neutral curve, induced by the modulation also change the curvature of $\varepsilon_0(q)$. At the minimum of the neutral curve the curvature is $\kappa = \partial^2 \varepsilon_0 / \partial q^2$ and with Eq. (29) one obtains the expression

$$\kappa = 2\xi_0^2 - \eta^2 \frac{16\bar{G}^2}{\xi_0^2 k^4} + \cdots . \tag{30}$$

These results are compared with the full numerical results for the threshold in Sec. 3.2.1.

3.1.2 Mean shift of the threshold for an ensemble of random functions $M(x)$

The sum in Eq. (23) may be further simplified by taking the average of it, because in this case the Fourier amplitudes can be eliminated by the correlation function of the Ornstein-Uhlenbeck process,

$$\langle \bar{c}_n \bar{c}_j^* \rangle = \frac{\bar{D}}{L(1 + \ell^2 (nk)^2)} \delta_{n,j} , \tag{31}$$

and with this expression, the mean shift of the threshold is

$$\langle \varepsilon_c^{(2)} \rangle = -\frac{\bar{D}L}{2\pi^2 \xi_0^2} \left(\frac{\pi^2}{6} - \sum_{n=1}^{\infty} \frac{(k\ell)^2}{1 + \ell^2 (nk)^2} \right) . \tag{32}$$

With the Digamma function $\psi(z)$ and the imaginary unit i, Eq. (32) may be rewritten in the following form

$$\langle \varepsilon_c^{(2)} \rangle = -\frac{\bar{D}L}{2\pi^2 \xi_0^2} \left(\frac{\pi^2}{6} + \frac{1}{2} ik\ell \left[\Psi(1 + \frac{i}{\ell k}) - \Psi(1 - \frac{i}{\ell k}) \right] \right) . \tag{33}$$

This mean value decreases linearly with the noise amplitude $\bar{D}$ and the reduction becomes smaller with increasing values of the coherence length ξ_0, i.e. systems with a large coherence length become rather insensitive against inhomogeneous perturbations of the control parameter. Also the inhomogeneous contribution $A_c^{(1)}(x)$ given by Eq. (22) decays as ξ_0^{-2}. A finite correlation length ℓ leads to a smaller threshold reduction, as indicated by the positive contribution of the ℓ-dependent second term in Eq. (32). The first part in Eq. (32) describes the threshold reduction in the limit of white noise, $\ell \to 0$, given by $\langle \varepsilon_c^{(2)} \rangle = -\bar{D}L/12\xi_0^2$. As indicated by Eq. (23) and Eq. (32) each mode

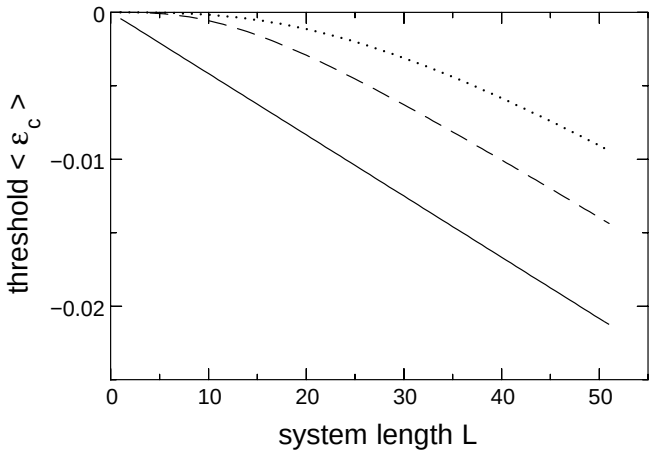

Fig. 1. The mean threshold according to formula (32) is plotted as a function of the system length L for a δ-correlated noise (solid line), and for random functions $\omega(x)$ with coherence length $\ell = \pi$ (dashed line) and $\ell = 2\pi$ (dotted line). The parameter values are $D = 0.02$ and $\xi_0 = 2$.

c_n of $M(x)$ contributes additively to the threshold reduction and the long–wavelength contributions dominate it. For finite values of ℓ, the dependence of the threshold on the length L is nonlinear, as indicated by the dashed and dotted lines in Fig. 1.

Using Eq. (21) and Eq. (31), one may estimate the validity range of the perturbation calculations, $\mid F_n^{(1)} \mid / F_n^{(0)} \ll 1$, and one obtains the following additional restriction with respect to the noise amplitude and system length

$$\sqrt{DL^3} \ll (2\pi)^2 \xi_0^2 \sqrt{1 + \ell^2 (2\pi/L)^2}\,. \tag{34}$$

This is further simplified for a δ-correlated noise to $\sqrt{DL^3} \ll (2\pi)^2 \xi_0^2$. Accordingly, one may expect deviations from the threshold shift $\langle \varepsilon_c^{(2)} \rangle$ as discussed above, as soon as the inequality in Eq. (34) is violated.

The variance of the threshold reduction is defined by $var(\varepsilon_c) = \langle \varepsilon_c^2 \rangle - \langle \varepsilon_c \rangle^2$ and for correlated noise the explicit expression of it is

$$var(\varepsilon_c) = \frac{4D^2}{L^2 \xi_0^4} \sum_{n=1}^{\infty} \frac{1}{(nk)^4 [1 + \ell^2 (nk)^2]^2}\ , \tag{35}$$

which may be further simplified in the case of white noise, i.e. $\ell \to 0$, to

$$var(\varepsilon_c) = \frac{D^2 L^2}{360\, \xi_0^4}\ . \tag{36}$$

This expression also indicates the trends of the threshold reduction in terms of the system length, the noise strength and the coherence length. Similar as

the mean value of the threshold, also the variance decreases with increasing values of the correlation length ℓ.

The ensemble average of the expression for the mean wave number in Eq. (27) yields

$$\langle q_m \rangle = \frac{Dk}{\pi \xi_0^4} \sum_{n=1}^{\infty} \frac{1}{(nk)^3[1+\ell^2(nk)^2]}\,, \tag{37}$$

which reduces for white noise to

$$\langle q_m \rangle = \frac{DL^2\zeta(3)}{4\xi_0^4\pi^3}\,, \tag{38}$$

with $\zeta(3) \approx 1.2$. With increasing values of the noise amplitude D higher order modes of the solution $A(x)$ become excited, which increases the mean wave number q_m. Conversely, the mean wave number q_m tends to zero when the noise amplitudes become smaller.

3.2 Numerical determination of the threshold

The trends, obtained by the perturbation calculation in the previous section, may be verified by a numerical solution of the linear part of Eq. (3) as described in this section. The Fourier expansion of $A(x)$, cf. Eq. (13), leads to the eigenvalue problem in Eq. (14). These coupled linear equations for the Fourier amplitudes may be rewritten in terms of a matrix equation $\mathcal{A}\mathbf{F} = \varepsilon\mathbf{F}$, where $\mathbf{F}$ includes the Fourier amplitudes F_j and $\mathcal{A}$ is the respective coefficient matrix

$$\mathcal{A} = \begin{pmatrix} \mathcal{L}_0(-N) & -c_1^* & \dots & \dots & 0 \\ -c_1 & \ddots & \ddots & \ddots & \vdots \\ \vdots & \ddots & \mathcal{L}_0(0) & \ddots & \vdots \\ \vdots & \ddots & \ddots & \ddots & -c_1^* \\ 0 & \dots & \dots & -c_1 & \mathcal{L}_0(N) \end{pmatrix} \tag{39}$$

with the abbreviation $\mathcal{L}_0(j) = \xi_0^2(jk)^2$. Since $\mathcal{A}$ is a hermitian matrix it has a real eigenvalue spectrum. The lowest eigenvalue of this set of $2N+1$ coupled equations provides the critical threshold ε_c either in the presence of a spatially periodic or a random modulation $M(x)$. By solving the linear problem for J realizations of $M(x)$, the shift of the mean value of the threshold $\langle \varepsilon_c \rangle$ is

obtained for each ensemble of realizations of $M(x)$. Since the long–wavelength contributions to $M(x)$ provide the major threshold reduction, as indicated by Eq. (32) and Fig. 4, already a medium number N of Fourier modes gives the threshold reduction with considerable accuracy.

The number of operations required for the numerical determination of the eigenvalues of $\mathcal{A}$ increases proportional to the number of Fourier modes as $\propto (2N+1)^3$. Therefore, for very large systems with $N \geq 10^3$ a direct numerical integration of the linear part of Eq. (3) by a pseudo-spectral method and studying the growth behavior of small perturbations becomes more efficient than determining the threshold ε_c by means of the eigenvalues of $\mathcal{A}$. Within this approach we start with arbitrary but small initial conditions for $A(x,t)$ and we detect the exponential growth behavior $\propto \exp(\lambda t)$ of the global quantity $N(t,\varepsilon) = 1/L \int_0^L dx\, A(x,t)^2$ as a function of ε. The threshold is determined when the growth rate λ changes its sign as a function of ε for each realization $M(x)$. This approach is very efficient in particular for large system lengths because in contrast to the eigenvalue problem, the number of operations increase only proportional to $Nlog(N)$ with the number of Fourier modes.

3.2.1 Harmonic modulation

The effects of a harmonic modulation $M(x) = 2G\cos(kx)$ on the threshold of a stationary bifurcation from the homogeneous state $A = 0$ are investigated first. In this case a truncation of the series in Eq. (13) to $N = 1$ with only three modes provides a useful analytical formula for the threshold ε_c

$$\varepsilon_c = \frac{1}{2}\xi_0^2 k^2 - \frac{1}{2}\sqrt{(\xi_0 k)^4 + 8G^2}\,, \tag{40}$$

which reduces in the limit of small modulation amplitudes $G \ll \xi_0^2 k^2$ to the result obtained by the perturbation calculation, cf. Eq. (24) . However, in the limit $k \to 0$, Eq. (40) approaches to the finite value $\varepsilon_c(k=0) = -\sqrt{2}G$, and there is no divergence as in the case of the perturbation calculation. This is also indicated in Fig. 2, where the wavenumber-dependence of the threshold according to Eq. (40) is shown by the dotted line. A full numerical solution gives in the limit $k \to 0$ the threshold shift $\varepsilon_c = -2G$, which is lower than that obtained by the three-mode approximation. Moreover, this value agrees with the threshold reduction obtained for a constant modulation function $M(x) = \max[2G\cos(kx)] = 2G$. The comparison in Fig. 2 between the full numerical results (solid line), the three mode approximation (dotted line) and the results of the perturbation calculation (dashed line) shows, that all three approaches provide similar results for larger values of the modulation wave number k, while there are for small values of k considerable deviations

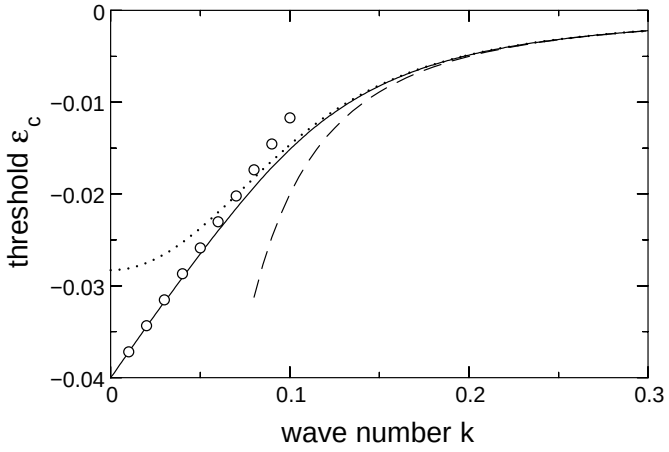

Fig. 2. The threshold reduction caused by a periodic modulation $M(x) = 2G\cos(kx)$ with $G = 0.02$ is shown as a function of the wave number k for different approximations. The dashed line is obtained by the perturbation calculation, cf. Eq. (24), the dotted line by the three mode ansatz, cf. Eq. (40), the solid line by the numerical solution for $N = 32$ modes and the formula given in Eq. (41) is indicated by the circles.

between the three approaches and the result of the perturbation calculation even diverges.

According to the $\pm x$ symmetry of the Ginzburg–Landau equation the threshold curve has a parabolic shape close to $k \sim 0$. However, apart from a narrow range around $k = 0$ the threshold obtained by the full numerical solution

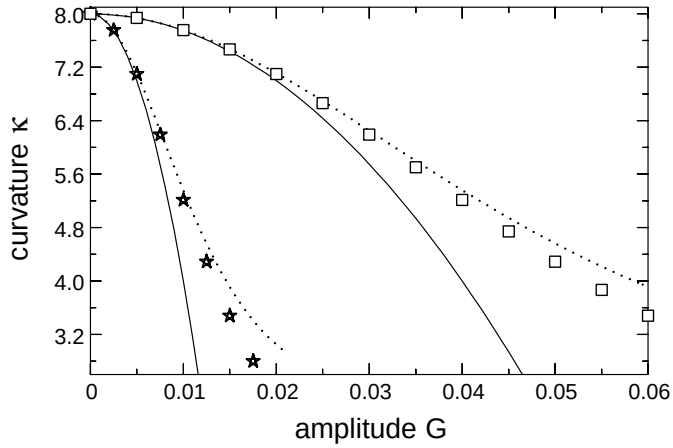

Fig. 3. The curvature $\kappa = \partial^2\varepsilon_0(q)/\partial q^2|_{q=0}$ of the neutral curve is shown as a function of the amplitude G for a harmonic modulation $M(x)$ and for two values of $k = 0.1,\ 0.2$. The solid line is due to the perturbation method, cf. Eq. (30), and the symbols are obtained by solving the eigenvalue problem numerically with $N = 64$ modes for $k = 0.2$ (squares) and $k = 0.1$ (stars). The dotted lines represent the results obtained by a three mode approximation similar as in Eq. (13). The coherence length is $\xi_0 = 2$.

follows in a wider range of k rather close a straight line, as indicated by the circles in Fig. 2, that are described by the formula

$$\varepsilon_c = -2G + \xi_0\sqrt{G}k \ . \tag{41}$$

The formula for smaller values of k together with the three mode approximation for larger values of k, cf. Eq. (40), approximate in a satisfying manner the threshold curve and also cover the parameter dependence of the threshold shift.

For $k = 0.2$ the results for the perturbation calculation and for the numerical solution are in rather good agreement, as can be seen in Fig. 2. However, there are already deviations for a smaller value $k = 0.1$. The curvature of the neutral curve, as determined by the perturbation method in Sec. 3.1.1, is also in agreement with the fully numerical solution for larger values of k and there are deviations at smaller values of k as shown in Fig. 3. The three mode approximation (dotted lines) reproduces roughly the curvature of the neutral curve even for larger values of G and k, where the perturbation calculation already deviates from the numerically exact solution.

3.2.2 Stochastic modulation

The threshold also depends on the spatial resolution of the random process $M(x)$. Below which spatial resolution $\Delta x = L/N$ and beyond which number of discretization points N becomes the mean threshold $\langle\varepsilon_c\rangle$ rather independent of N for a fixed system length L? For a δ-correlated random function $\xi(x)$ on a discrete lattice with a constant site distance Δx the values of $\xi(x)$ at x_i and $x_i + \Delta x$ are statistically independent. However, a finite site distance Δx mimics a finite correlation length. When this length is not very small compared to the coherence length ξ_0 and the system length L, the threshold for a given noise strength obviously depends on the discretization Δx and therefore on the number of sites N. This is illustrated in Fig. 4, where the averaged threshold is shown as a function of Δx for a system of length $L = 64\pi$. It can be seen that for $Nk/2 \gtrsim 3$, corresponding to $\Delta x \leq \pi/3$ the mean value of the threshold reduction is nearly independent of N and this estimate of Δx can also be used for systems of a different length $L = 2\pi/k$.

In part (a) of Fig. 5 the mean threshold reduction $\langle\varepsilon_c\rangle$ is shown as a function of the system length L for a fixed discretization Δx and in part (b) as a function of the noise amplitude D for a δ-correlated noise process. The solid lines show the results obtained by the perturbation calculation, cf. Eq. (32). The inset in part (b) shows the threshold shift in the range of small values of D, where the result of the perturbation calculation is of fairly good agreement with the full numerical one. Both approaches deviate from each other with increasing values

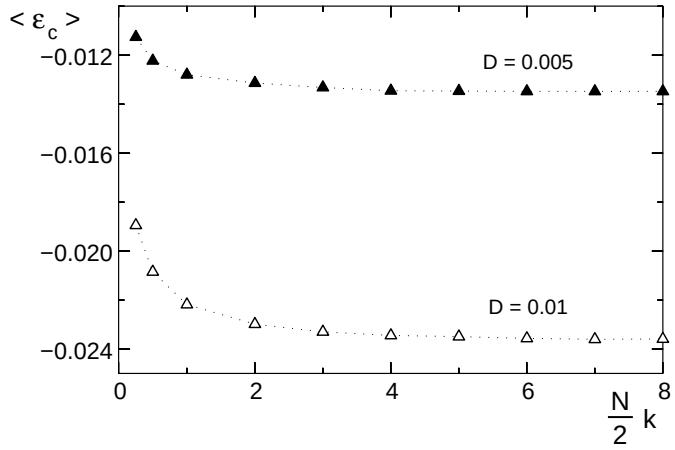

Fig. 4. The averaged threshold $\langle \varepsilon_c \rangle$ is shown for a fixed system $L = 64\pi = 2\pi/k$ and for two values of the noise amplitude D as a function of the Fourier modes N and the discretization Δx, respectively. The evaluation of the ensemble averages are calculated from $20,000$ realizations of a δ-correlated $M(x)$.

of D and L, respectively, because of the increasing ratio $A_c^{(1)}/A_c^{(0)}$, which is a measure for the violation of the assumption of the perturbation calculation, cf. Eq. (34). The top parts in Figs. 5(a) and 5(b) show the respective standard deviation σ_{ε_c}

$$var(\varepsilon_c) \equiv \sigma_{\varepsilon_c}^2 = \langle\, \varepsilon_c^2 \,\rangle - \langle\, \varepsilon_c \,\rangle^2 \ . \tag{42}$$

Again, for rather small values of L and D the standard deviation σ_{ε_c} is also well described by the result of the perturbation calculation given by Eq. (36).

The threshold reduction saturates with increasing values of the system length L, as indicated in Fig. 6(a). In addition, the variance reaches at a system length of about $L = 100 \sim 50\xi_0$ a maximum and beyond this length, it decays as a function of L as shown in Fig. 6(b) for two different values of the noise amplitude D. These tendencies may be interpreted as follows. The results in Fig. 4 show that below some discretization length Δx, which depends especially on the coherence length ξ_0, the threshold becomes rather independent with respect to further refinements of the discretization. So keeping Δx fixed at a finite value, but increasing the system length and the number of sites N, the uniformly distributed random numbers are increasingly explored. With an increasing system length, it becomes more likely that the random number ξ_j given by Eq. (10) hits the most positive value $\sqrt{12D/\Delta x}\ /2$ and with the next neighbors $\xi_{j\pm n}$ also in the positive range. In such a case a considerable threshold reduction can be achieved, which is limited from below by $-\sqrt{12D/\Delta x}\ /2$, a value, that is obtained for a constant modulation $\xi_j = \sqrt{12D/\Delta x}\ /2$ for $j = 0, \ldots, N$. In that respect, the tendencies shown in Fig. 6 corresponds to a close exploration of the lower boundary of the threshold.

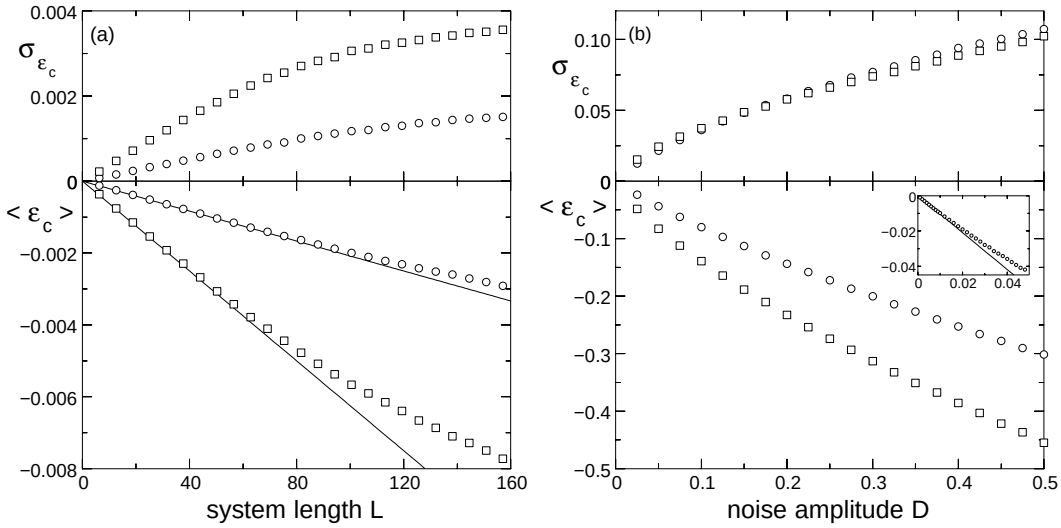

Fig. 5. In part (a) the mean threshold $\langle \varepsilon_c \rangle$ decreases as a function of the system length L and in part (b) as a function of the noise amplitude D. The inset in part (b) displays $\langle \varepsilon_c \rangle$ in the range of small values of D while the solid line represents the threshold shift given by Eq. (32) for $\ell = 0$. The top parts show the standard deviation σ_{ε_c}. Parameters in part (a) are $D = 0.001$ (circles) and $D = 0.003$ (squares) and in part (b) $L = 16\pi$ (circles) and $L = 64\pi$ (squares). 20,000 realizations of $\xi(x)$ with $\Delta x \approx 0.39$ have been used to evaluate the ensemble averages.

The variance $var(\varepsilon_c)$ decreases for large values of L as shown in Fig. 6(b) and this decay follows roughly a power law as $\propto L^{-\nu}$, where the curves shown in this figure are fitted (solid lines) with the exponents $\nu \approx 0.18$ for $D = 0.05$ and $\nu \approx 0.2$ for $D = 0.1$. Both curves are in rather good agreement with the numerics and they indicate in the limit $L \to \infty$ a vanishing variance for the

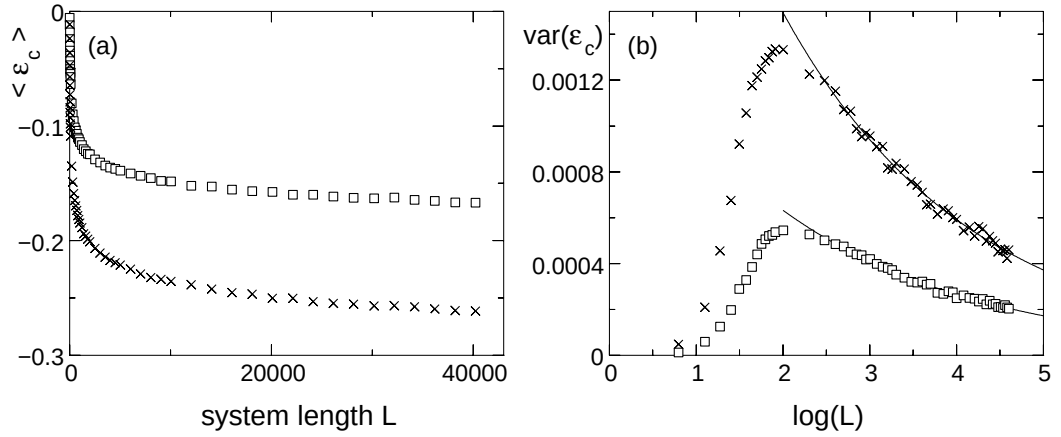

Fig. 6. In part (a) the mean threshold and in part (b) its variance are shown for δ-correlated noise as a function of the system length L up to rather large values. The parameters are $D = 0.05$ (squares), $D = 0.1$ (crosses), $\xi_0 = 2$, $J = 1,000$ and $\Delta x \approx 0.785$. The solid lines represent fit curves of the form $var(\varepsilon_c) \propto L^{-\nu}$ with the exponents $\nu \approx 0.18$ for $D = 0.05$ and $\nu \approx 0.2$ for $D = 0.1$.

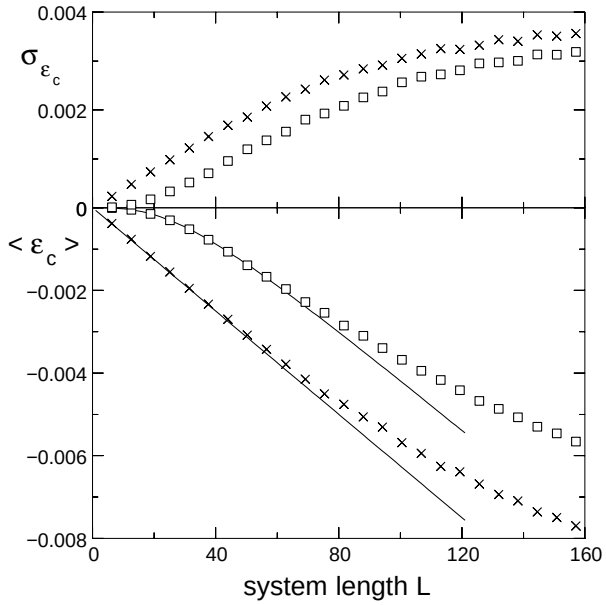

Fig. 7. The threshold reduction (bottom) and the standard deviation (top) are plotted for colored noise with $\ell = 2\pi$ (squares) and for white noise (crosses) as functions of the system length L and for the noise amplitude $D = 0.003$. The solid lines show the threshold shifts according to the expression given by Eq. (32) for the respective correlation length ℓ. The discretization $\Delta x \approx 0.19$ and $J = 10,000$ realizations of $M(x)$ have been used.

critical control parameter.

The effect of a finite correlation length ℓ is shown in Fig. 7, where we compare the mean value of the threshold as a function of the system length for random functions with a vanishing correlation length $\ell = 0$ (crosses) and one with $\ell = 2\pi$ (squares). This figure shows, that the threshold reduction and its variance are smaller for a finite correlation length ℓ than for $\ell = 0$. This is also indicated by the result of the perturbation calculation given in Eq. (32) (solid lines in Fig. 7).

Another interesting statistical quantity is the distribution of the threshold, i.e. the probability $P(\varepsilon_c)d\varepsilon$ to find for a single realization of the random function $M(x)$ the threshold in a small interval $(\varepsilon_c, \varepsilon_c + d\varepsilon)$. This distribution function is shown in Fig. 8 for different values of the system length L and for the noise strength $D = 0.001$. Due to the asymmetry of the distribution there is no coincidence between the most probable threshold ε_c^m, determined by $max\,[P(\varepsilon_c)]$, and the mean threshold $\langle\varepsilon_c\rangle$, indicated as dotted lines in this figure. The maximum of the distribution $P(\varepsilon_c)$ is reduced with the system length while its width increases. This is in agreement with the standard deviation σ_{ε_c} shown in Fig. 5(a) (top part) or with the result of the perturbation calculation, cf. Eq. (36). For very long systems, however, the distribution $P(\varepsilon_c)$ becomes narrower and the maximum of $P(\varepsilon_c)$ at ε_c^m increases, which is in agreement

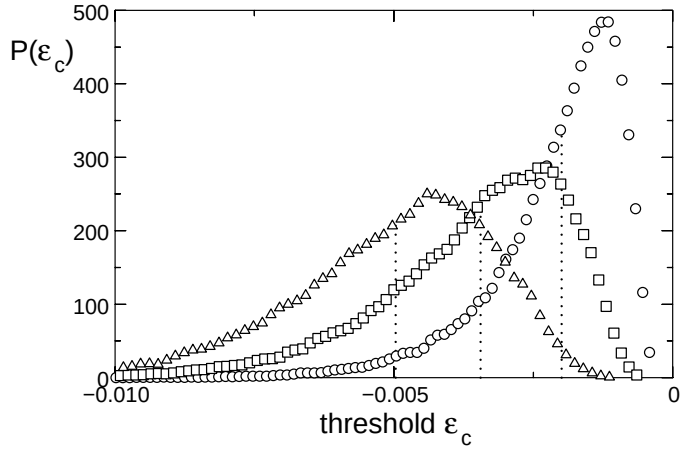

Fig. 8. Distribution function $P(\varepsilon_c)$ for the threshold is shown for three different values of the system length: $L = 32\pi$ (circles), $L = 64\pi$ (squares), and $L = 128\pi$ (triangles). The noise amplitude is $D = 0.001$ and the distribution of the thresholds ε_c has been calculated for $J = 50,000$ realizations of the δ–correlated random function $M(x)$. The dotted lines indicate the respective mean value $\langle \varepsilon_c \rangle$ of the threshold.

with the decreasing variance of ε_c in Fig. 6(b) for $L \geq 200$.

In the absence of the modulation ($M = 0$), the eigensolution $A(x)$ of the linear part of Eq. (3) is either a constant function for $\varepsilon = \varepsilon_c$ or it is a harmonic function $\propto \exp(iqx)$ along the neutral curve $\varepsilon_0 = \xi_0^2 q^2$. With an increasing amplitude of the random function $M(x)$, the eigenfunction at threshold becomes more and more spatially localized as shown in Fig. 9(a), whereby one realization of the random function itself is shown at the bottom of this figure. This increasing localization is also indicated by the power spectrum of the eigenfunctions in Fig. 9(b), which becomes broader for more localized functions, i.e. with increasing noise strength higher order modes are excited. This tendency also leads to a larger mean wave number of the eigenfunction as given by Eq. (37). The large amplitude of the constant mode F_0 is not included in Fig. 9(b). The eigenfunctions are normalized, i.e. $1/L \int_0^L dx\, A^2 = 1$.

The eigenfunctions corresponding to larger eigenvalues of $\mathcal{A}$ than the critical one and therefore to larger values of the threshold, exhibit a similar localized behavior, but their peaks are located in different regions within the given system length L. This localization behavior of the eigenfunctions of $\mathcal{A}$ is important for the nonlinear bifurcation behavior of the amplitude equation, which is discussed in Sec. 4 in greater detail. For a random function with a finite correlation length ℓ, all the eigenfunctions of $\mathcal{A}$ become less pronounced with increasing values of ℓ.

The spatial correlation $\langle A(x + x_1)A(x) \rangle$ of the eigenfunctions of $\mathcal{A}$ averaged over a sequence of realizations of $M(x)$ decays with increasing values of the

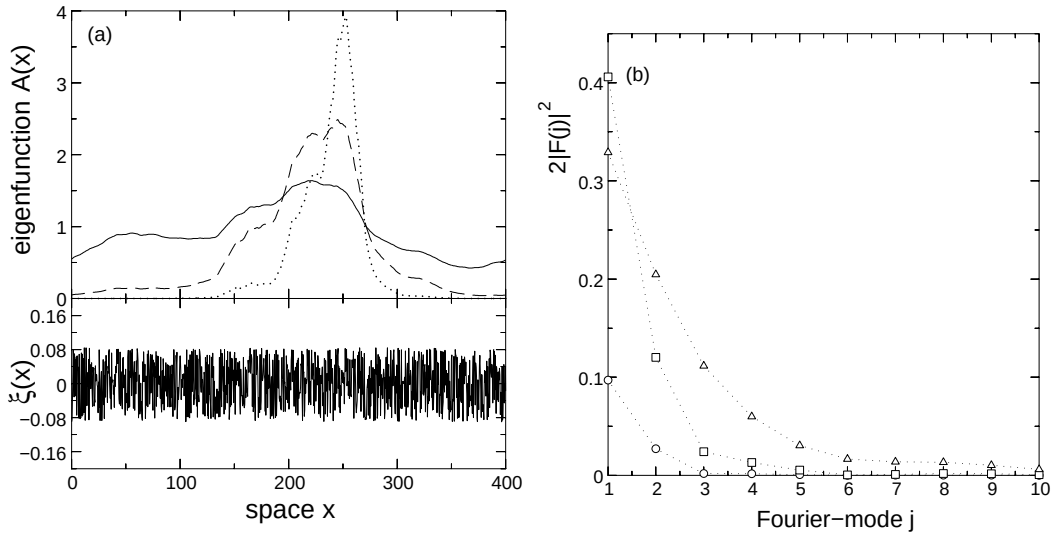

Fig. 9. In part (a) the spatial dependence of the eigenfunction $A(x)$ at threshold $\varepsilon = \varepsilon_c$ is shown for the noise amplitudes $D = 10^{-4}$ (solid line), $D = 10^{-3}$ (dashed line) and $D = 10^{-2}$ (dotted line) and for one realization of the random function $\xi(x)$, illustrated for $D = 10^{-3}$ by the bottom part on a grid with $\Delta x \approx 0.39$. Part (b) shows the amplitudes F_j of the three eigenfunctions in part (a), whereby $D = 10^{-4}$ (circles), $D = 10^{-3}$ (squares), and $D = 10^{-2}$ (triangles). The large constant mode F_0 is not included.

displacement x_1 as shown in Fig. 10 for δ–correlated noise and for different values of the noise amplitude. The typical decay length of this correlation function decreases with increasing values of the noise amplitude D, indicating that for larger values of D the randomness is transferred to the spatial form of the solution $A(x)$. On the other hand, increasing the noise amplitude D enforces the regions, where $A(x)$ becomes very small and therefore the contribution of such regions to the correlation function becomes small too.

3.3 Self-consistent approximation scheme

With a self-consistent iteration scheme, we describe in this section a third method for solving the linear part of Eq. (3). The technique is inspired by a Greens-function method used in turbulence [42], which reads in its discrete formulation as follows. One starts with the coupled equations for the Fourier-amplitudes given in Eq. (14). Since the constant contribution to $M(x)$ vanishes, i.e. $c_0 = 0$, we split the equations for F_0 and F_j with $j \neq 0$. For $j = 0$, Eq. (14) takes the form

$$\varepsilon_c F_0 + \mathbf{C}^* \mathbf{D} = 0\,, \tag{43}$$

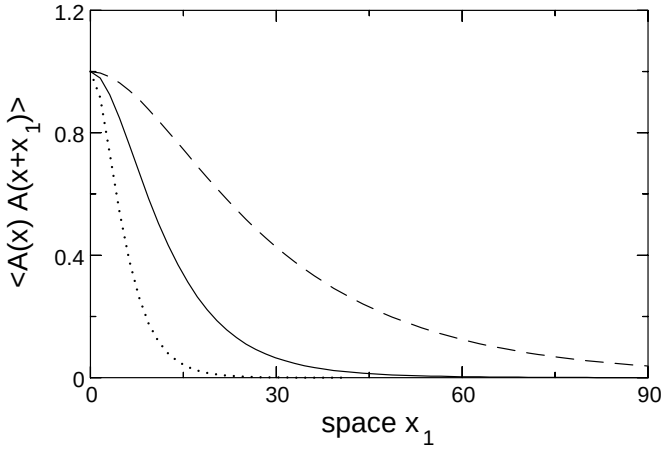

Fig. 10. The spatial correlation function $\langle A(x)A(x+x_1)\rangle$ of the eigenfunction at threshold is shown as a function of the displacement x_1 for a δ-correlated noise and for three different values of the noise strength: $D = 0.01$ (solid line), $D = 0.1$ (dashed line), and $D = 1$ (dotted line). The ensemble average has been calculated from $J = 1,000$ realizations of the stochastic process $M(x)$ for a system of length $L = 128\pi$ with grid space $\Delta x \approx 0.39$.

where the unknown vector $\mathbf{D}$ and the vector $\mathbf{C}$ of the noise amplitudes

$$\begin{aligned} \mathbf{D} &= \left(F_{-N/2+1}, \ldots, F_{-1}, F_1, \ldots, F_{N/2}\right) \ , \\ \mathbf{C} &= \left(c_{-N/2+1}, \ldots, c_{-1}, c_1, \ldots, c_{N/2}\right) \ , \end{aligned} \tag{44}$$

include $N-1$ components with the index $-N/2+1$ to $N/2$ but not F_0 and c_0, respectively. The vector $\mathbf{D}$ is determined by the following inhomogeneous linear equation

$$\mathcal{B}_0\mathbf{D} = \mathcal{B}_1\mathbf{D} + F_0\mathbf{C} \ , \tag{45}$$

which includes the $N-1$ equations for $j \neq 0$ given in Eq. (14). Herein the two matrices $\mathcal{B}_0$ and $\mathcal{B}_1$ of dimension $(N-1)\times(N-1)$ are defined by

$$\begin{aligned} \mathcal{B}_{0_{ij}} &= \left[\xi_0^2(jk)^2 - \varepsilon_c\right]\ \delta_{i,j} \ , \\ \mathcal{B}_{1_{jl}} &= c_{j-l}, \qquad\qquad \text{with} \qquad -N/2+1 \leq j-l \leq N/2 \, . \end{aligned} \tag{46}$$

In addition, the matrix $\mathcal{B}_1$ has due to the vanishing component $c_0 = 0$ no elements on its diagonal. The $N-1$ components of the unknown vector $\mathbf{D}$ may be determined by the iteration scheme

$$\mathbf{D}_{n+1} = \mathcal{B}_0^{-1}\left(\mathcal{B}_1\mathbf{D}_n + F_0\mathbf{C}\right) \ , \tag{47}$$

with the initial condition $\mathbf{D}_0 = 0$. Using the n-th iteration as an approximate solution $\mathbf{D} = \mathbf{D}_{n+1}$ then one obtains with the help of Eq. (43) the following equation

$$\varepsilon_c + \mathbf{C}^* \left[\sum_{i=0}^{n}\left(\mathcal{B}_0^{-1}\mathcal{B}_1\right)^i\right]\mathcal{B}_0^{-1}\mathbf{C} = 0 \, , \tag{48}$$

for the determination of the critical control parameter ε_c. This equation may be solved numerically either for a periodic or a single realization of the stochastic modulation of the control parameter. In order to calculate the mean value $<\varepsilon_c>$ for an ensemble of realizations of $M(x)$, this equation has to be solved either J times or an equation for the mean value $<\varepsilon_c>$ may be derived as described below.

3.3.1 The limiting case of small modulation amplitudes

Restricting the iteration scheme in Eq. (48) to $n = 0$, the equation

$$\varepsilon_c - \sum_n{}' \frac{|c_n|^2}{\varepsilon_c - \xi_0^2 (nk)^2} = 0\,, \tag{49}$$

that may be solved by a standard numerical routine, determines the threshold approximately. If we assume in Eq. (49) small modulation amplitudes $|c_n|^2 = \eta^2 |\bar{c}_n|^2$ with $\eta \ll 1$ and $\varepsilon_c \propto \eta^2 \ll \xi_0^2 k^2$, then the resulting expression for ε_c becomes in leading order of η identical with the result of the perturbation calculation given in Eq. (23).

3.3.2 The equation for the mean value $<\varepsilon_c>$

One motivation for introducing the iteration method in this work is the possibility to derive for the average $<\varepsilon_c>$ itself an equation. In such a case, the averaged statistical properties of the noise can be used instead of solving the threshold problem for J different realizations of $M(x)$ before averaging.

However, by taking for instance the average of Eq. (49) directly, one has to deal with the expression $\langle |c_n|^2/(\varepsilon_c - \xi_0^2 (nk)^2)\rangle$ that includes the ratio of the two random processes $|c_n|^2$ and ε_c. Here, we approximate the statistical average of this ratio by assuming their statistical independence and replacing it by the ratio of their averages. In this case an equation for $\langle \varepsilon_c \rangle$ follows:

$$\langle \varepsilon_c \rangle - \frac{Dk}{2\pi} \sum_j{}' \frac{1}{[1 + \ell^2 (jk)^2]\,[\langle \varepsilon_c \rangle - \xi_0^2 (jk)^2]} = 0\ . \tag{50}$$

An extension of such a decomposition to higher orders of the iteration scheme in Eq. (48) becomes rather cumbersome because of the $(n+2)$-point correlation functions with respect to c_j. For instance, for an iteration order up to $n = 2$ one has to deal in Eq. (48) with the decomposition of a four-point correlation function into a sum of two-point correlation functions: $\langle c_i^* c_j c_n c_m \rangle = \langle c_i^* c_j \rangle \langle c_n c_m \rangle + \langle c_i^* c_n \rangle \langle c_j c_m \rangle + \langle c_i^* c_m \rangle \langle c_j c_n \rangle$. The uneven $(2n+1)$-point correlation functions do not contribute to the threshold, because their ensemble

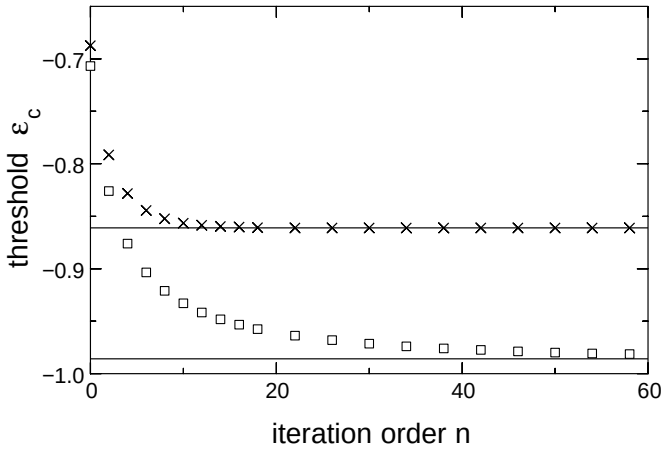

Fig. 11. The convergence of the threshold as a function of the iteration order n in Eq. (48) is shown for a periodic modulation $M(x) = 2G\cos(kx)$ with the amplitude $G = 0.5$ and wave numbers $k = 0.1$ (crosses) and $k = 0.01$ (squares). The solid line describes the threshold obtained by the numerical scheme given in Sec. 3.2.

averages vanish in Eq. (48). The expression corresponding to Eq. (50), but expanded up to the order $n = 2$ has been solved too and the corresponding result is given in Fig. 14.

Taking for $\ell = 0$ the limit $k \to 0$ in Eq. (50), corresponding to a system of infinite length L, the sum may be transformed into an integral. The latter one can be easily evaluated and one obtains the saturation value for the mean threshold

$$\langle \varepsilon_c \rangle = -\left(\frac{D}{2\xi_0}\right)^{2/3} , \tag{51}$$

similar as for the three mode approximation for a harmonic modulation in Eq. (40) and in contrast to the perturbation calculation.

3.3.3 Numerical results for the iteration scheme

The convergence of the iteration scheme (48) as a function of the iteration order n is shown for a periodic modulation $M(x) = 2G\cos(kx)$ in Fig. 11 for two different values of the wave number $k = 0.01,\ 0.1$ and for the modulation amplitude $G = 0.5$. The solid lines describe the thresholds calculated via Eq. (14) for many modes. The iteration order n that is necessary for a reasonable approximation of the threshold depends on the modulation parameters and it converges faster for larger values of k and smaller values of G, similar as for the perturbation calculation in Sec. 3.1.

The convergence of the iteration scheme for one realization of a random func-

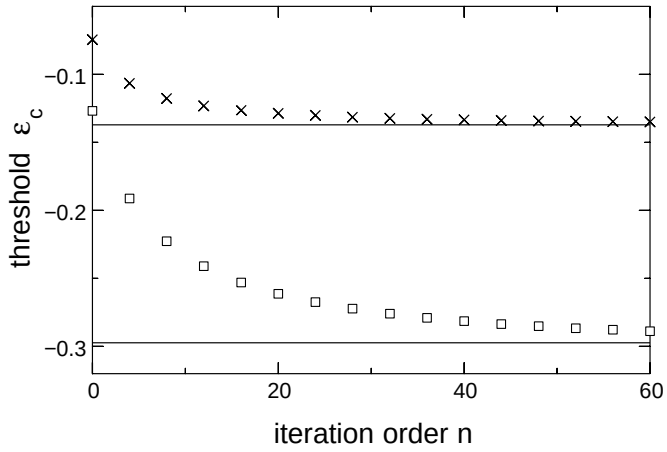

Fig. 12. For the system length $L = 200\pi$ ($\equiv k = 0.01$), the convergence of the threshold ε_c is shown as a function of the iteration order n for two realizations of a δ-correlated noise with $\Delta x \approx 0.39$ and noise amplitudes $D = 0.08$ (crosses), $D = 0.13$ (squares). The solid lines describe the threshold obtained for the same realization by determining the lowest eigenvalues of $\mathcal{A}$.

tion $M(x)$ but for two different amplitudes D is shown in Fig. 12. The convergence as a function of n is similar as for a periodic modulation with $k = 0.01$, corresponding to the same system length $L = 200\pi$. Since $M(x)$ is composed of short- and long-wavelength contributions, the long-wavelength contributions determine obviously the convergence of the iteration scheme. Therefore, in the presence of a random function $M(x)$ the convergence depends very much on the system size and according to Fig. 12 also on the noise amplitudes.

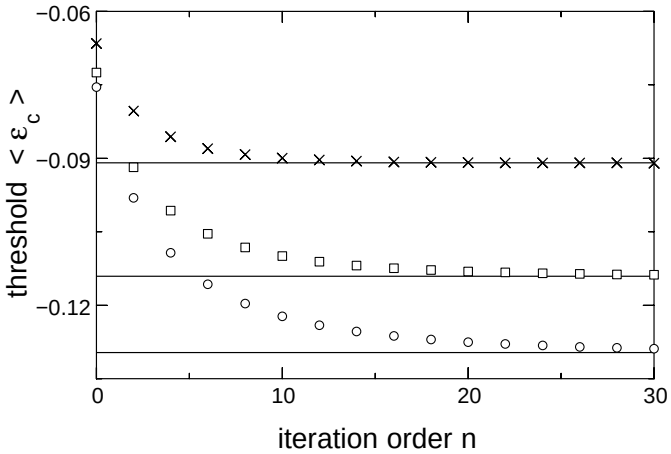

Fig. 13. The mean threshold $\langle \varepsilon_c \rangle$ is shown as a function of the iteration order n for three different lengths: $L = 10\pi$ (crosses), $L = 15\pi$ (squares), $L = 20\pi$ (circles). The amplitude of the δ–correlated noise is $D = 0.1$ and $\Delta x \approx 0.785$. The averages have been determined by $J = 1,000$ realizations of the random function $M(x)$. The solid lines are obtained by calculating the lowest eigenvalues of the matrix $\mathcal{A}$ for the same random processes.

In Fig. 13 instead of the threshold for one realization, the mean value of the threshold $\langle \varepsilon_c \rangle$ is shown as a function of the iteration order n for an ensemble of δ-correlated random functions $M(x)$ with noise strength $D = 0.1$ and for different values of L. Again, the convergence becomes slower with increasing system size and higher iteration orders n are required in order to approach to the mean threshold calculated with eigenvalues of $\mathcal{A}$. Since the matrices $\mathcal{B}_i$ have the same dimension as the matrix $\mathcal{A}$, the latter one may become numerically more efficient for single realizations because of the high number of iterations n required for longer systems.

As described above, in long systems and for a large noise amplitude an iteration of Eq. (48) up to large values of n is required in order to obtain a reasonable approximation of the threshold. This disadvantage may be compensated when a solution for J realizations can be avoided and an equation for the mean value of the threshold $\langle \varepsilon_c \rangle$ can be derived similar as in Eq. (50). In such a case the equations must be solved only once, which reduces the computational effort considerably. However, the derivation of an equation for the mean value $\langle \varepsilon_c \rangle$ becomes rather cumbersome for higher orders of the iteration scheme, because of the $(n+2)$-point correlation functions that have to be decomposed into a series of two-point correlation functions.

In addition, the assumption that $|c_n|^2$ and ε_c are independent random variables is used in this scheme. For the iteration order $n = 0$ we have verified the related error. The dashed line in Fig. 14 is obtained by solving Eq. (50) and

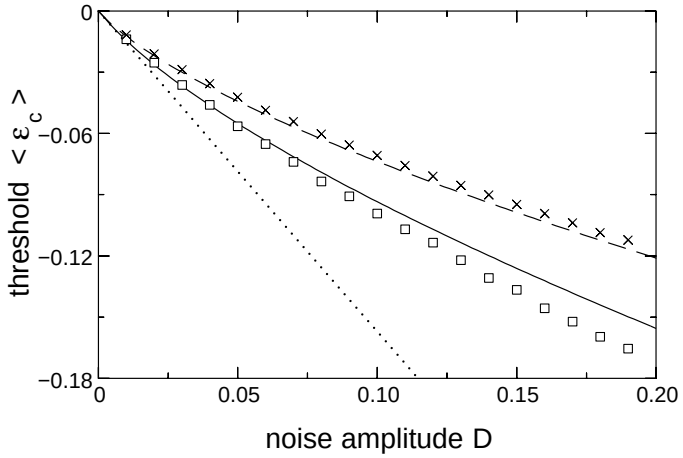

Fig. 14. The mean threshold $\langle \varepsilon_c \rangle$ calculated by four different approaches is shown as a function of the noise amplitude D of a δ–correlated noise. The dashed line is the mean value $\langle \varepsilon_c \rangle$ determined by Eq. (50) and the solid line is obtained by a formula corresponding to Eq. (50) but extended up to the iteration order $n = 2$. The dotted line represents the perturbation calculation, the squares correspond to the full numerical result for the threshold and the crosses indicate the threshold obtained by taking the average of $J = 10,000$ solutions of Eq. (48) for $n = 0$. The system length is $L = 24\pi$.

the crosses in this figure are obtained by solving Eq. (48) at leading iteration order $n = 0$ for J realizations of the random function $M(x)$ and calculating the average. The small difference between these two lines indicates that only a small error is made by assuming $|c_n|^2$ and ε_c as independent random variables. The same assumption together with the decomposition of a four-point correlation function was used at the iteration order $n = 2$ and the result is shown in Fig. 14 by the solid line, which is already rather close to the full solution (squares).

4 Nonlinear behavior

The nonlinear solutions of Eq. (3) are investigated in this section, where we start in Sec. 4.1 with a few selected numerical results in order to estimate some trends imposed by the modulation $M(x)$. Any finite parametric modulation $M(x)$ reduces the threshold as shown in Sec. 3 and in addition, it induces (strongly) modulated solutions. On the other hand, for large values $\varepsilon \gg M(x)$ the effects related to $M(x)$ become small and accordingly, a transition range as a function of ε may be expected, which increases with the noise amplitude D. These trends are investigated in more detail in Sec. 4.2 by a perturbation expansion, which is valid immediately above the threshold, and further beyond threshold by another expansion around the homogeneous nonlinear solution in Sec. 4.3.

In order to characterize the stationary and nonlinear, but inhomogeneous solutions of Eq. (3), we introduce a global order parameter $N(\varepsilon)$ defined by the integral for a system of length L

$$N(\varepsilon) = \frac{1}{L} \int_0^L dx \ \mid A(x) \mid^2 \ . \tag{52}$$

In terms of thermal convection, $N(\varepsilon)$ describes the so–called *Nusselt number*. Besides the mean wave number q_m introduced by Eq. (26), we introduce with

$$q_m^o = \frac{\sum_j |q_j||F_j|^2}{\sum_j{}' |F_j|^2} \ , \tag{53}$$

a further wave number for a characterization especially of the spatially varying portion of $A(x)$ for each realization $M(x)$ as well as the variance of it $var(q_m^o) = \langle {q_m^o}^2 \rangle - \langle q_m^o \rangle^2$. Here, the acute brackets again denote an ensemble average and F_j are the amplitudes of the Fourier representation of $A(x)$. The prime at the sum of the denominator in Eq. (53) means that the index $j = 0$ and therefore the dominating amplitude $F_0 \sim \sqrt{\varepsilon/g}$ of the constant contribution is excluded. By neglecting this term the expression in Eq. (53)

is a measure for the mean wave number of the spatially varying part of $A(x)$ around the constant solution $A^2 = \varepsilon/g$. Also the coherence length defined by

$$\Xi = \left(\frac{\sum_j (|q_j| - q_m^o)^2 \, |F_j|^2}{\sum_j |F_j|^2} \right)^{-1/2} , \tag{54}$$

will be rather useful for a characterization. Without the inhomogeneity $M(x)$, the nonlinear stationary solution of Eq. (3) is $A(x) = \sqrt{(\varepsilon - \xi_0^2 q^2)/g} \;\; \exp(iqx)$ and one has in this case a linear ε-dependence of $N(\varepsilon) = (\varepsilon - \xi_0^2 q^2)/g$ for $\varepsilon > 0$ and a vanishing N below threshold.

4.1 Numerical results

The nonlinear Eq. (3) is solved by a standard pseudo-spectral code and since we are mainly interested in stationary solutions $A(x)$, the simulation time is chosen sufficiently long to reach the respective stationary state.

For a large number of realizations of a δ-correlated random function $M(x)$, one of it is shown by the lower part in Fig. 9(a), we have calculated the mean value of $N(\varepsilon)$ as well as the mean wave number $\langle q_m^o \rangle$ and its variance as functions of the control parameter ε for various noise amplitudes $D = 0.01$ (circles), $D = 0.04$ (squares) and $D = 0.25$ (crosses) as shown in Fig. 15(a)-(c). The solution $A(x)$ is given in part (e) for one realization of $M(x)$ and for four different values of the control parameter $\varepsilon = -0.016,\ 0.01,\ 0.1,\ 0.5$. With increasing values of ε the spatially varying portion of $A(x)$ becomes smaller and the spatially independent part becomes dominating. Simultaneously, the short–wavelength contributions to the spatially varying portion of $A(x)$ become larger compared to the long–wavelength ones and the spatial localization becomes weaker. Both tendencies determine the major trends of the nonlinear behavior of $\langle N(\varepsilon) \rangle$, that of the averaged wave number $\langle q_m^o \rangle$ and its variance $var(q_m^o)$ as well as of the mean coherence length $\langle \Xi \rangle$ as shown in Fig. 15(a)-(d).

Even for a finite modulation amplitude the function $N(\varepsilon)$ still approaches at large values of ε the straight line in Fig. 15(c), which is obtained in the unmodulated limit, $M(x) = 0$, because the spatially varying portion of $A(x)$ decreases with increasing values of ε, cf. Fig. 15(e). On the other hand, all finite modulations $M(x)$ reduce the threshold, as shown in the previous section and therefore, $A(x)$ and $N(\varepsilon)$ are already finite at negative values of ε. As a consequence of this earlier take off and of the approach of $N(\varepsilon)$ to the curve of the unmodulated case for large values of the control parameter ε, the slope $\frac{dN(\varepsilon)}{d\varepsilon}|_{\varepsilon=\varepsilon_c}$ at threshold decreases with increasing amplitudes of $M(x)$ while the curvature $\frac{d^2N(\varepsilon)}{d\varepsilon^2}|_{\varepsilon=\varepsilon_c}$ increases. The parameter dependence of both quantities is discussed in greater detail in terms of a perturbation calculation in Sec. 4.2.

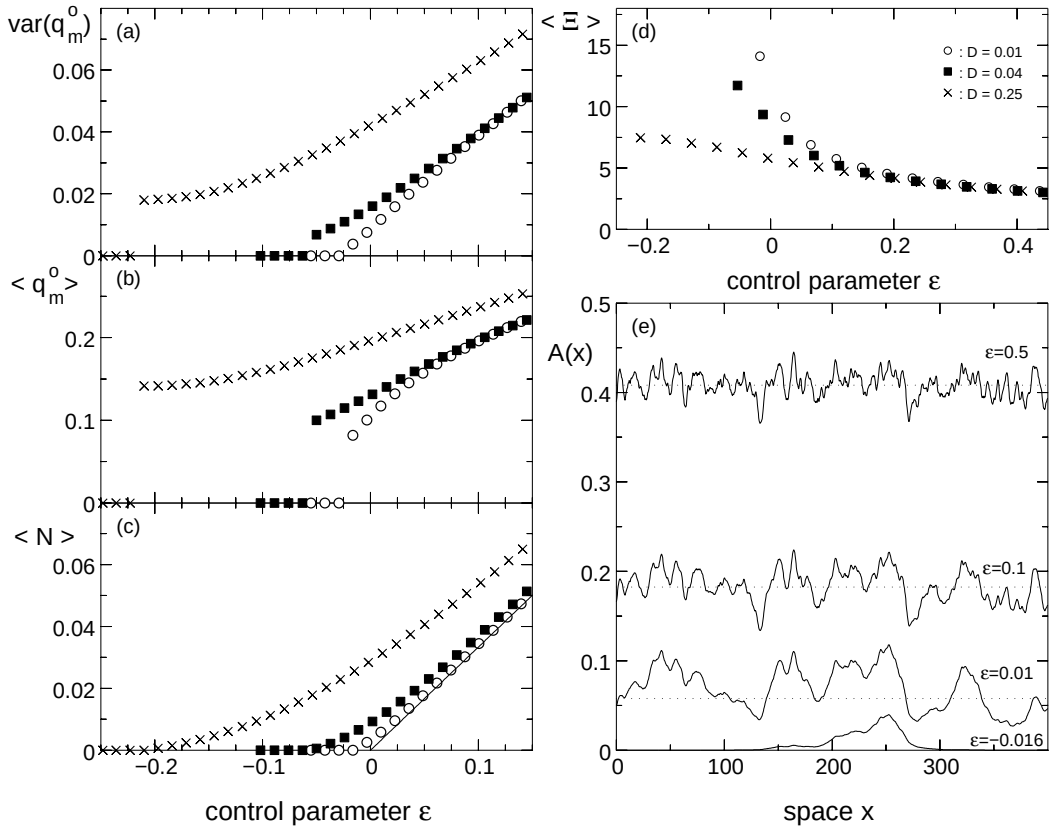

Fig. 15. In part (a) the mean squared deviation $var(q_m^o)$, in parts (b) and (c) the mean values of q_m^o and $N(\varepsilon)$ are shown as a function of ε for different values of the noise amplitude: $D = 0.01$ (circles), $D = 0.04$ (squares) and $D = 0.25$ (crosses). The solid line in part (c) indicates the unperturbed linear behavior of $N(\varepsilon) = \varepsilon/g$ for $g = 3$. Part (d) shows the mean coherence length $\langle \Xi \rangle$ given by Eq. (54) as a function of ε. The system length is $L = 32\pi$ and the averages have been evaluated by using 100 realizations of a δ-correlated random function $M(x)$ with $\Delta x \approx 0.39$. The averaged threshold values are $\langle \varepsilon_c \rangle = -1.637 \times 10^{-2}$ for $D = 0.01$, $\langle \varepsilon_c \rangle = -5.144 \times 10^{-2}$ for $D = 0.04$ and $\langle \varepsilon_c \rangle = -0.21$ for $D = 0.25$. In part (e) the nonlinear solutions $A(x)$ of Eq. (3) are shown for various values of ε and for a single realization of the random function $M(x)$ with a noise amplitude $D = 0.01$.

At threshold, the mean wave number $\langle q_m^o \rangle$ also increases with the noise amplitude D but at large values of ε, $\langle q_m^o \rangle$ becomes rather independent of D, as indicated in Fig. 15(b). The latter tendency has its origin in the decay of the coherence length as a function of ε, as shown in Fig. 15(d). The short–wavelength contributions, being suppressed by a larger coherence length close to threshold, can emerge at large values of ε, where Ξ becomes small for any noise amplitude D. This has to be compared with the behavior of the mean wave number $\langle q_m \rangle$, as defined in Eq. (26), which becomes small in the limit of a small noise amplitude D and large values of ε, because in both limits the spatially constant contribution F_0 is dominating and therefore the amplitude of the wavenumber q_c of the real field $u(x,t)$ in Eq. (1).

Immediately above threshold the Poincaré - Lindstedt expansion [43] is used for the determination of $A(x)$ and $N(\varepsilon)$ as well as of its slope $dN(\varepsilon)/d\varepsilon|_{\varepsilon=\varepsilon_c}$ and its curvature $d^2N(\varepsilon)/d\varepsilon^2|_{\varepsilon=\varepsilon_c}$. The basic solution $A \equiv 0$ of the modified Ginzburg-Landau equation loses its stability already at a threshold in the negative range, $\varepsilon_c(\eta) < 0$, as determined in the previous section, where η was used as a measure for the strength of the modulation amplitude $M(x)$. Both, the order parameter A and the control parameter ε are expanded with respect to a small parameter λ that measures the distance from $\varepsilon_c(\eta)$ and the small amplitude of A close to threshold:

$$A(x) = \frac{1}{\sqrt{g}} \left[\lambda A_1(x) + \lambda^2 A_2(x) + \lambda^3 A_3(x) + \ldots \right] \ , \tag{55a}$$

$$\varepsilon - \varepsilon_c(\eta) = \lambda\varepsilon_1 + \lambda^2\varepsilon_2 + \lambda^3\varepsilon_3 + \lambda^4\varepsilon_4 \ldots \ . \tag{55b}$$

We focus with this ansatz on stationary solutions and therefore we will neglect the time derivative in Eq. (3). With the formulas in Eqs. (55) the model in Eq. (3) may be expanded with respect to powers of λ. This leads to a hierarchy of equations, similar as in Sec. 3.1, from which all the corrections A_j and ε_j are determined by using the Fredholm solubility condition.

The equation obtained at the leading order of λ is

$$\mathcal{L}_\eta A_1(x) = 0 \tag{56}$$

with the self-adjoint operator

$$\mathcal{L}_\eta = \varepsilon_c(\eta) + \eta\bar{M}(x) + \xi_0^2\partial_x^2 \, . \tag{57}$$

For $\eta = 0$ this becomes the unperturbed operator given in Eq. (18) and the fact that $A_1(x)$ belongs to the kernel of the operator $\mathcal{L}_\eta$ is crucial for the determination of the higher order corrections ε_j and A_j by the equations at higher order in λ in this hierarchy. Equation (56) was also the starting point for the determination of the threshold $\varepsilon_c(\eta)$ as discussed in Sec. 3.1. In order to get analytical expressions for the coefficients of the Poincaré - Lindstedt expansion we will later on restrict η to small values and determine the first correction A_1 by using the results of that section.

At order λ^2 the following inhomogeneous equation is obtained

$$\mathcal{L}_\eta A_2(x) = -\varepsilon_1 A_1(x) \ . \tag{58}$$

According to the Fredholm theorem this equation is solvable if the inhomogeneity of the right hand side is orthogonal to the solution of the adjoint operator $\mathcal{L}_\eta^\dagger$. This condition requires that the leading correction in ε vanishes

$$\varepsilon_1 = 0 \,, \tag{59}$$

and Eq. (58), which becomes homogeneous as Eq. (56) may be solved by $A_2 = \gamma A_1$ with a real constant γ.

At the next higher order λ^3, one again obtains an inhomogeneous equation

$$\mathcal{L}_\eta A_3(x) = -\varepsilon_2 A_1(x) + |A_1(x)|^2 A_1(x) \,. \tag{60}$$

Using the Fredholm condition this equation gives the first nontrivial correction to ε

$$\varepsilon_2 = \frac{(A_1, |A_1|^2 A_1)}{(A_1, A_1)} \,, \tag{61}$$

where $(.,.)$ denotes the canonical scalar product. Once the solution $A_1(x)$ of Eq. (56) has been found, ε_2 is also known. At fourth order in λ the equation

$$\mathcal{L}_\eta A_4(x) = -\varepsilon_3 A_1 - \varepsilon_2 A_2 + A_1^2 A_2^* + 2|A_1|^2 A_2 \,, \tag{62}$$

is obtained. Applying the solubility condition to Eq. (62) and using the relation $A_2 = \gamma A_1$ together with Eq. (60) leads to the following relations

$$\varepsilon_3 = 2\gamma\varepsilon_2 \qquad \text{and} \qquad \mathcal{L}_\eta A_4 = 3\gamma \mathcal{L}_\eta A_3 \,, \tag{63}$$

where the latter equation is obviously solved by

$$A_4 = 3\gamma A_3 \,. \tag{64}$$

The solubility condition applied to the equation at order λ^5 yields

$$\varepsilon_4 = \widetilde{\varepsilon}_4(\gamma = 0) + \gamma^2 \varepsilon_2 \tag{65}$$

with

$$\widetilde{\varepsilon}_4 = \frac{(A_1, A_1^2 A_3^*)}{(A_1, A_1)} + 2\frac{(A_1, A_3 |A_1|^2)}{(A_1, A_1)} - \varepsilon_2 \frac{(A_1, A_3)}{(A_1, A_1)} \,. \tag{66}$$

Using $\varepsilon_1 = 0$ together with Eq. (55b), λ may be eliminated from Eq. (55a) so that

$$A(x) = \frac{1}{\sqrt{g}} \left(\frac{\varepsilon - \varepsilon_c}{\varepsilon_2}\right)^{1/2} A_1 + \frac{1}{\sqrt{g}} \left(\frac{\varepsilon - \varepsilon_c}{\varepsilon_2}\right) \left[A_2 - \frac{\varepsilon_3}{2\varepsilon_2} A_1\right] + \frac{1}{\sqrt{g}} \left(\frac{\varepsilon - \varepsilon_c}{\varepsilon_2}\right)^{3/2} \left[A_3 - \frac{\varepsilon_3}{\varepsilon_2} + \frac{5\varepsilon_3^2}{8\varepsilon_2^2} - \frac{\varepsilon_4}{2\varepsilon_2} A_1\right] + O\left(\frac{\varepsilon - \varepsilon_c}{\varepsilon_2}\right)^2 \tag{67}$$

follows. With the expressions for ε_3, A_4 and ε_4, as determined above, it turns out that this expression for $A(x)$ is independent of the constant γ. Accordingly, $\gamma = 0$ and therefore $\varepsilon_3 = A_4 = A_2 = 0$ may be chosen. In this case $A(x)$ takes an even simpler form

$$A(x) = \frac{1}{\sqrt{g}} \left(\frac{\varepsilon - \varepsilon_c}{\varepsilon_2}\right)^{1/2} A_1 + \frac{1}{\sqrt{g}} \left(\frac{\varepsilon - \varepsilon_c}{\varepsilon_2}\right)^{3/2} \left[A_3 - \frac{\varepsilon_4}{2\varepsilon_2} A_1\right] + O\left(\frac{\varepsilon - \varepsilon_c}{\varepsilon_2}\right)^{5/2} , \tag{68}$$

where we have dropped the tilde of ε_4. Equation (68) is the final result of the Poincaré-Lindstedt expansion of $A(x)$ up to order $(\varepsilon - \varepsilon_c)^{3/2}$ and the Nusselt number in terms of $A(x)$ is in leading order of $\lambda^2 = (\varepsilon - \varepsilon_c)/\varepsilon_2$

$$N(\varepsilon) = \frac{1}{L} \int_0^L dx\, |A(x)|^2 = (A(x), A(x)) = \frac{\lambda^2}{g} (A_1, A_1) + \frac{\lambda^4}{g} \left[(A_1, A_3) + (A_3, A_1) - \frac{\varepsilon_4}{\varepsilon_2}(A_1, A_1)\right] + \dots . \tag{69}$$

In order to obtain explicit analytical expressions for $N(\varepsilon)$ as well as for the slope $\partial_\varepsilon N$ and the curvature $\partial_\varepsilon^2 N$ at threshold as a function of the parameters, one has to determine the explicit form of the corrections A_i as described in the next subsection.

4.2.1 Determination of the coefficients of the Poincaré–Lindstedt expansion

The starting point of the determination of A_j and ε_j is the expansion with respect to small modulation amplitudes η as already introduced in Sec. 3.1

$$A_1 = F_0 + \eta A_c^{(1)} + \eta^2 A_c^{(2)} + \dots . \tag{70}$$

Here F_0 is an undetermined amplitude that will drop out in the final expressions of $N(\varepsilon)$, cf. Secs. 4.2.2 and 4.2.3. The first correction $A_c^{(1)}$, as given by

Eq. (22), is due to the relation $c_{-n} = c_n^*$ for the Fourier amplitudes of the modulation $M(x)$ a real function.

According to Eqs. (70) and (61) one obtains for ε_2

$$\varepsilon_2 = F_0^2 + 5\,\eta^2(A_c^{(1)}, A_c^{(1)}) + O(\eta^4)\ , \tag{71}$$

and due to the inhomogeneity in Eq. (60), the expansion of A_3 starts in leading order $\propto \eta$. Therefore, we choose the ansatz

$$A_3(x) = \eta A_3^{(1)}(x) + \eta^2 A_3^{(2)}(x) + \dots\ , \tag{72}$$

and with Eq. (60) in leading order of η the inhomogeneous real equation

$$\left(\varepsilon_c^{(0)} + \xi_0^2\partial_x^2\right) A_3^{(1)}(x) = 2F_0^2 A_c^{(1)}(x)\ , \tag{73}$$

follows and therefore $A_3^{(1)}$ is a real function as well.

The correction ε_4 given by Eq. (66) is in leading order of η

$$\varepsilon_4 = 8\,\eta^2(A_c^{(1)}, A_3^{(1)}) + O(\eta^4)\,. \tag{74}$$

With all these expressions for the coefficients in Eq. (68), one ends up for $A(x)$ with

$$\begin{aligned} A(x) = &\frac{(\varepsilon-\varepsilon_c)^{1/2}}{\sqrt{g}}\left(1 + \eta\frac{A_c^{(1)}}{F_0} + \eta^2\left[\frac{A_c^{(2)}}{F_0} - \frac{5(A_c^{(1)}, A_c^{(1)})}{2F_0^2}\right]\right) \\ &+ \frac{(\varepsilon-\varepsilon_c)^{3/2}}{\sqrt{g}}\left(\eta\frac{A_3^{(1)}}{F_0^3} + \frac{\eta^2}{2F_0^4}\left[2F_0A_3^{(2)} - 8(A_c^{(1)}, A_3^{(1)})\right]\right) + \dots\ . \end{aligned} \tag{75}$$

For a vanishing modulation, i.e. $\eta = 0$ and therefore $\varepsilon_c = 0$, the well known behavior of a supercritical bifurcation $A \propto \sqrt{\varepsilon}$ follows.

The expansion of $N(\varepsilon)$ as given in Eq. (69) takes now the following form:

$$N(\varepsilon) = (\varepsilon-\varepsilon_c)\ s(\eta) + (\varepsilon-\varepsilon_c)^2\ \kappa(\eta) + O(\varepsilon-\varepsilon_c)^3\ , \tag{76}$$

with the abbreviations for the slope $s(\eta) = \frac{dN(\varepsilon)}{d\varepsilon}|_{\varepsilon=\varepsilon_c}$

$$s(\eta) = \frac{1}{g}\left(1 - \eta^2\frac{4}{F_0^2}\left(A_c^{(1)}, A_c^{(1)}\right)\right) + O(\eta^4)\ , \tag{77}$$

and the curvature $2\kappa(\eta) = \frac{d^2N(\varepsilon)}{d\varepsilon^2}|_{\varepsilon=\varepsilon_c}$

$$\kappa(\eta) = -\eta^2 \frac{6}{F_0^4 g} \left(A_c^{(1)}, A_3^{(1)} \right) + O(\eta^4) \ . \tag{78}$$

Both the slope and the curvature are explicitly calculated for a periodic and stochastic function $M(x)$ in the following two subsections.

4.2.2 Analytic results for periodic modulations

At first, we consider a periodic modulation of the control parameter $M(x) = \eta \bar{M}(x) = 2G\cos(Qx)$ with the amplitude $G = \eta \bar{G}$ and wave number Q. The function $A_c^{(1)}$ is obtained by using the Fourier modes of the modulation $M(x)$ in Eq. (22) and $A_3^{(1)}$ is obtained by solving Eq. (73). For both one obtains

$$A_c^{(1)} = \frac{2\bar{G}F_0}{\xi_0^2 Q^2} \cos(Qx) \qquad \text{and} \qquad A_3^{(1)} = -\frac{4\bar{G}F_0^3}{\xi_0^4 Q^4} \cos(Qx) \ . \tag{79}$$

Using these solutions as well as the expressions for $s(\eta)$ and $\kappa(\eta)$ the function $N(\varepsilon)$ up to second order is

$$N(\varepsilon) = \frac{(\varepsilon - \varepsilon_c)}{g} \left(1 - \eta^2 \frac{8\bar{G}^2}{\xi_0^4 Q^4} \right) + \eta^2 \frac{(\varepsilon - \varepsilon_c)^2}{g} \frac{24\bar{G}^2}{\xi_0^6 Q^6} + O(\varepsilon - \varepsilon_c)^3 \ . \tag{80}$$

From Eq. (80) the slope and curvature of $N(\varepsilon)$ with respect to the control parameter ε follows immediately

$$\left. \frac{\partial N(\varepsilon)}{\partial \varepsilon} \right|_{\varepsilon_c} = \frac{1}{g} \left(1 - \eta^2 \frac{8\bar{G}^2}{\xi_0^4 Q^4} \right) \qquad \text{and} \tag{81a}$$

$$\left. \frac{\partial^2 N(\varepsilon)}{\partial \varepsilon^2} \right|_{\varepsilon_c} = \eta^2 \frac{48\bar{G}^2}{g \xi_0^6 Q^6} \ . \tag{81b}$$

The slope of $N(\varepsilon)$ at threshold decreases with increasing values of the modulation amplitude $\propto G^2$, while the curvature of $N(\varepsilon)$ increases at threshold proportional G^2. This is consistent since a smaller slope of $N(\varepsilon)$ at ε_c requires a larger curvature, because $N(\varepsilon)$ has for any modulation amplitude a similar slope at large values of ε. Note that the curvature is always positive.

4.2.3 Analytic results for stochastic modulations

For a randomly varying function $M(x)$ the solutions $A_c^{(1)}$ and $A_3^{(1)}$ are calculated in a similar way as for a periodic modulation and the solutions are given by

$$A_c^{(1)} = \sum_{n=-\infty}^{\infty}{}' \frac{F_0 \bar{c}_n}{\xi_0^2 (nk)^2} e^{inkx} \qquad \text{and} \qquad A_3^{(1)} = -\sum_{n=-\infty}^{\infty}{}' \frac{2F_0^3 \bar{c}_n}{\xi_0^4 (nk)^4} e^{inkx} \; . \tag{82}$$

With these expressions together with the definition of $s(\eta)$ and $\kappa(\eta)$ the function $N(\varepsilon)$ takes the form

$$\begin{aligned} N(\varepsilon) = & \frac{(\varepsilon - \varepsilon_c)}{g} \left(1 - 4\eta^2 \sum_{n=-\infty}^{\infty}{}' \frac{|\bar{c}_n|^2}{\xi_0^4 (nk)^4} \right) \\ & + 12 \frac{(\varepsilon - \varepsilon_c)^2}{g} \eta^2 \sum_{n=-\infty}^{\infty}{}' \frac{|\bar{c}_n|^2}{\xi_0^6 (nk)^6} + O(\varepsilon - \varepsilon_c)^3 \, . \end{aligned} \tag{83}$$

The prime at the sum excludes the index $n = 0$ and therefore the deviations of $N(\varepsilon)$ from the linear behavior only depend on the noise amplitudes $|c_n|^2$. Since ε_c depends itself on the realization of the power spectrum $|c_n|^2$, an ensemble average of $N(\varepsilon)$ is not possible with a decomposition of the product of the two stochastic processes ε_c and $|c_n|^2$. However, the ensemble averages of the first and second derivative of $N(\varepsilon)$ can be specified, because here only the second moment of the noise enters. Accordingly, one obtains for the mean value of the slope

$$\left\langle \left. \frac{\partial N(\varepsilon)}{\partial \varepsilon} \right|_{\varepsilon_c} \right\rangle = \frac{1}{g} \left(1 - 8\eta^2 \sum_{n=1}^{\infty} \frac{< |\bar{c}_n|^2 >}{\xi_0^4 (nk)^4} \right) \; , \tag{84}$$

and for the mean curvature

$$\left\langle \left. \frac{\partial^2 N(\varepsilon)}{\partial \varepsilon^2} \right|_{\varepsilon_c} \right\rangle = \eta^2 \, \frac{48}{g} \sum_{n=1}^{\infty} \frac{< |\bar{c}_n|^2 >}{\xi_0^6 (nk)^6} \; . \tag{85}$$

Taking the explicit expressions for the second moments of the noise with amplitude $D = \eta^2 \bar{D}$, one obtains for correlated noise

$$\left\langle \left. \frac{\partial N(\varepsilon)}{\partial \varepsilon} \right|_{\varepsilon_c} \right\rangle = \frac{1}{g} \left(1 - \frac{4\eta^2 \bar{D} k}{\pi \xi_0^4} \sum_{n=1}^{\infty} \frac{1}{(nk)^4 [1 + \ell^2 (nk)^2]} \right) \qquad \text{and} \tag{86a}$$

$$\left\langle \left. \frac{\partial^2 N(\varepsilon)}{\partial \varepsilon^2} \right|_{\varepsilon_c} \right\rangle = \eta^2 \, \frac{24 \bar{D} k}{\pi \xi_0^6 g} \sum_{n=1}^{\infty} \frac{1}{(nk)^6 [1 + \ell^2 (nk)^2]} \; . \tag{86b}$$

and in the limiting case of white noise

$$\left\langle \left. \frac{\partial N(\varepsilon)}{\partial \varepsilon} \right|_{\varepsilon_c} \right\rangle = \frac{1}{g}\left(1 - \eta^2 \frac{\bar{D}L^3}{180\,\xi_0^4}\right) \qquad \text{and} \tag{87a}$$

$$\left\langle \left. \frac{\partial^2 N(\varepsilon)}{\partial \varepsilon^2} \right|_{\varepsilon_c} \right\rangle = \eta^2 \frac{\bar{D}L^5}{1260\,\xi_0^6 g}\ . \tag{87b}$$

Similar as for a periodic modulation of the control parameter, the slope at threshold is reduced with increasing noise amplitudes and the positive curvature of $N(\varepsilon)$ increases with D.

Using the results for the corrections $A_c^{(1)}$ and $A_3^{(1)}$ as given in Eq. (82) the mean wave number as defined by Eq. (26) can also be expanded for small values of η and as a function of the distance from threshold $\varepsilon - \varepsilon_c$. One obtains

$$q_m = 2\eta^2 \sum_{n=1}^{\infty} \left(\frac{|\bar{c}_n|^2}{\xi_0^4 (nk)^3} - 4\frac{(\varepsilon - \varepsilon_c)}{g} \frac{|\bar{c}_n|^2}{\xi_0^6 (nk)^5} + 4\frac{(\varepsilon - \varepsilon_c)^2}{g} \frac{|\bar{c}_n|^2}{\xi_0^8 (nk)^7} \right) \tag{88}$$

and at threshold $\varepsilon = \varepsilon_c$ the mean wave number is recovered, as given by Eq. (27). The ensemble averages of both the slope and the curvature of q_m at threshold are

$$\left\langle \left. \frac{\partial q_m(\varepsilon)}{\partial \varepsilon} \right|_{\varepsilon_c} \right\rangle = -\frac{8\eta^2}{g} \sum_{n=1}^{\infty} \frac{\langle |\bar{c}_n|^2 \rangle}{\xi_0^6 (nk)^5} \qquad \text{and} \tag{89a}$$

$$\left\langle \left. \frac{\partial^2 q_m(\varepsilon)}{\partial \varepsilon^2} \right|_{\varepsilon_c} \right\rangle = \frac{16\eta^2}{g} \sum_{n=1}^{\infty} \frac{\langle |\bar{c}_n|^2 \rangle}{\xi_0^8 (nk)^7}\ . \tag{89b}$$

The formulas for white or correlated noise follow by inserting the respective correlation function. The finite value of the mean wave number at threshold as well as its negative slope and positive curvature show that $\langle q_m \rangle$ decreases with increasing values of the control parameter. This is in contrast to the wave number q_m^o as defined in Eq. (53). The decay of $\langle q_m \rangle$ reflects the increasingly dominating contribution of the homogeneous state $|F_0|^2 \propto \varepsilon$ that has been neglected in the expression of q_m^o, but dominates now for large values for ε.

4.2.4 Numerical results of the Poincaré - Lindstedt expansion

In Fig. 16 the slope $\frac{dN(\varepsilon)}{d\varepsilon}|_{\varepsilon=\varepsilon_c}$ and the curvature $\frac{d^2N(\varepsilon)}{d\varepsilon^2}|_{\varepsilon=\varepsilon_c}$ are shown for a periodic modulation $M(x) = 2G\cos(Qx)$ as a function of the modulation amplitude G and for two different values of the modulation wave number Q. Both the decreasing behavior of the slope and the increasing nature of the curvature as functions of G, as predicted by the formulas in Eqs. (81), agree with the results obtained by numerical simulations, especially for small values of the modulation wave number. Both trends indicate an increasing

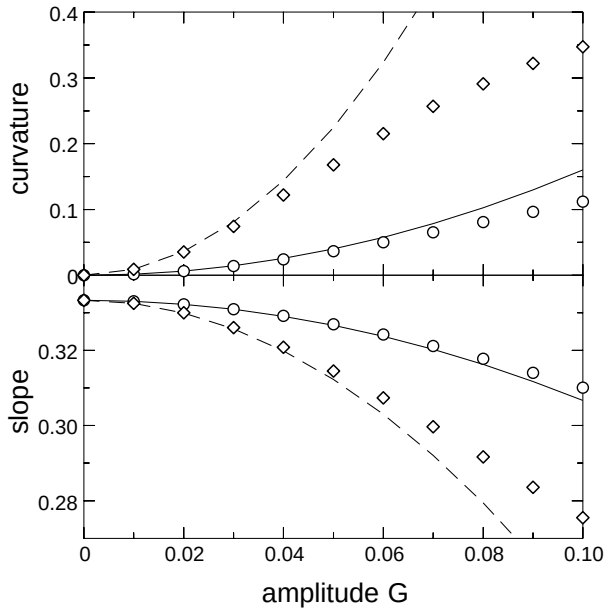

Fig. 16. The slope $\frac{dN(\varepsilon)}{d\varepsilon}|_{\varepsilon=\varepsilon_c}$ and curvature $\frac{d^2N(\varepsilon)}{d\varepsilon^2}|_{\varepsilon=\varepsilon_c}$ of $N(\varepsilon)$ at threshold are displayed for a periodic modulation $M(x) = 2G\cos(Qx)$ as a function of the modulation amplitude G for two different wave numbers $Q = 0.5$ (circles) and $Q = 0.375$ (diamonds). The solid and the dashed lines are plots of the respective formula of the Poincaré-Lindstedt expansion given by Eqs. (81).

transition range with G from the lowered threshold to the linear behavior of $N(\varepsilon)$ further beyond the threshold. The perturbation calculation and the numerical simulations are again closer for larger values of the modulation wave number Q, similar as the decreasing difference between the full numerical solution and the perturbation approach with increasing values of Q in Sec. 3.

The effects of a random modulation $M(x)$ on the slope and the curvature of $N(\varepsilon)$ are shown Fig. 17 for a system of length $L = 16\pi$ and two different values of the correlation length $\ell = 0$ in part (a) and $\ell = \pi$ in part (b). Similar as for the shift of the threshold in Sec. 3, the agreement between the results from the perturbation expansion and from the numerical calculations are best at small values of the modulation amplitude D. The range of agreement increases with decreasing system lengths and vice versa. In Figs. 16 and 17 the analytically predicted slope is smaller and the predicted curvature is larger than those obtained by the numerical solution of the model equation, but this is also consistent with the stronger reduction of the threshold as obtained by the perturbation calculation.

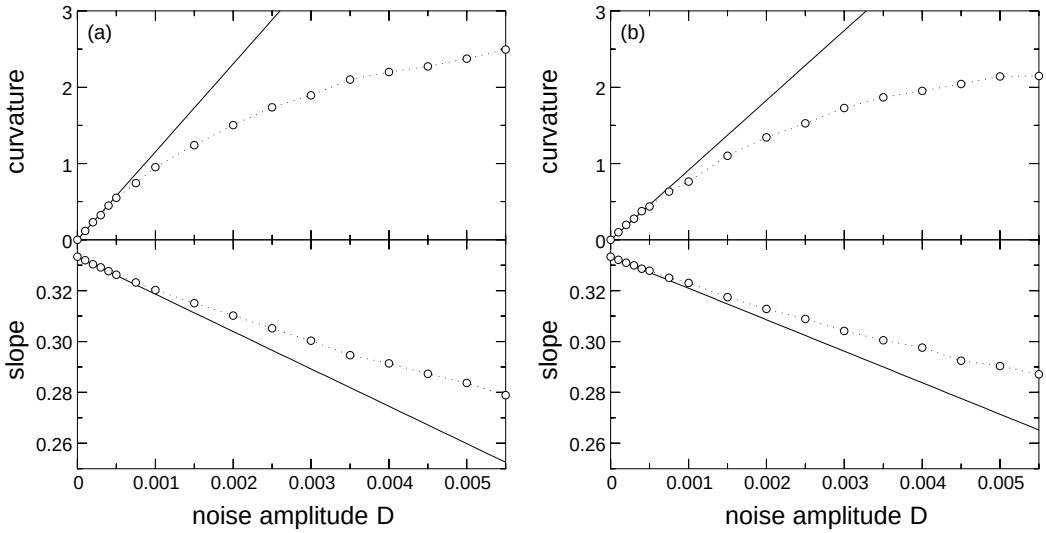

Fig. 17. The average of the slope $\langle \frac{dN(\varepsilon)}{d\varepsilon}|_{\varepsilon=\varepsilon_c} \rangle$ and of the curvature $\langle \frac{d^2N(\varepsilon)}{d\varepsilon^2}|_{\varepsilon=\varepsilon_c} \rangle$ of $N(\varepsilon)$ at threshold are shown as a function of the noise amplitude D for a δ-correlated noise in part (a) and for a colored noise with correlation length $\ell = \pi$ in part (b). The system length is in both cases $L = 16\pi$ and the grid space is $\Delta x \approx 0.39$. The averages from numerical simulations were calculated in terms of $1,000$ realizations of the random function $M(x)$. The solid lines represent the results according to the Poincaré-Lindstedt expansion given for white noise by Eqs. (87) and for colored noise by Eqs. (86).

4.3 Expansion of $A(x)$ with respect to deviations from $\sqrt{\varepsilon/g}$

The partial differential equation (3) has for $M(x) = 0$ a constant nonlinear solution $A_0^2 = \varepsilon/g$. For small modulations $M(x) = \eta\bar{M}(x)$ with $\eta \ll 1$, and the ansatz

$$A = \frac{1}{\sqrt{g}}\Big[A_0 + \eta A_1 + \eta^2 A_2 + \dots\Big] \ . \tag{90}$$

Eq. (3) may be expanded with respect to powers η up to order η^2,

$$\eta^0 : (\varepsilon + \xi_0^2\partial_x^2)A_0 - \mid A_0 \mid^2 A_0 = 0 \ , \tag{91a}$$

$$\eta^1 : (\varepsilon + \xi_0^2\partial_x^2)A_1 - (2A_1 + A_1^*)\, A_0^2 = -\bar{M}(x)A_0 \ , \tag{91b}$$

$$\eta^2 : (\varepsilon + \xi_0^2\partial_x^2)A_2 - (2A_2 + A_2^*)\, A_0^2 = -\bar{M}(x)A_1 + A_0\left(A_1^2 + 2 \mid A_1 \mid^2\right) \ . \tag{91c}$$

and from this hierarchy of equations the corrections A_i may determined. The solution of Eq. (91a) is given by the constant $A_0^2 = \varepsilon$ or by the periodic function $A_0(x) = \sqrt{\varepsilon - \xi_0^2 q^2}\ \exp(iqx)$. The solution of Eq. (91b) is

$$A_1(x) = \sum_{n=-\infty}^{\infty} a_n e^{inkx}\,, \tag{92}$$

whereby the Fourier coefficients

$$a_n = \frac{A_0}{\xi_0^2(nk)^2 + 2\varepsilon}\ \bar{c}_n \tag{93}$$

are determined by the Fourier amplitudes of $\bar{M}(x) = \sum_n \bar{c}_n \exp(inkx)$. Note that the constant contribution $a_0 = 0$ vanishes according to the vanishing mean value of $M(x)$ and that for large values of ε the first order contribution $A_1(x) \propto 1/\sqrt{\varepsilon}$ becomes small. To evaluate $N(\varepsilon)$ as defined in Eq. (52) up to order η^2, we only need the spatially independent contribution of $A_2(x)$, which is given by

$$\tilde{A}_2 = \frac{A_0}{2\varepsilon} \sum_{n=-\infty}^{\infty} \frac{|\bar{c}_n|^2[\xi_0^2(nk)^2 - \varepsilon]}{[\xi_0^2(nk)^2 + 2\varepsilon]^2}\ , \tag{94}$$

and which also becomes small for large values of ε. Together with the spatially independent contribution $|\tilde{A}_1|^2$ of $|A_1|^2$, the Nusselt number $N(\varepsilon)$ may be expanded with respect to the noise amplitude η as follows

$$N(\varepsilon) = \frac{1}{L}\int_0^L dx\ \mid A \mid^2 = \frac{1}{g}\Big[A_0^2 + \eta^2(2A_0\tilde{A}_2 + |\tilde{A}_1|^2) + \ldots\Big] \tag{95}$$

and with the explicit expressions for A_i Eq. (95) takes the compact form

$$N(\varepsilon) = \frac{1}{g}\Big[\varepsilon + \eta^2 \sum_{n=-\infty}^{\infty} \frac{\xi_0^2(nk)^2|\bar{c}_n|^2}{[\xi_0^2(nk)^2 + 2\varepsilon]^2} + \ldots\Big]\ . \tag{96}$$

Equation (96) describes the behavior of $N(\varepsilon)$ beyond the threshold ε_c. In the vicinity of the threshold of the bifurcation, ε becomes of the order η^2 and may be neglected in the denominator in Eq. (96). Therefore N vanishes precisely at the negative threshold given in Eq. (23). This holds both for deterministic and stochastic modulations of the control parameter. Far beyond threshold the contribution of the modulation to N vanishes as $1/\varepsilon^2$ and the Nusselt number approaches the linear ε-dependence of the unperturbed situation in agreement with the trend indicated by the full numerical solution shown in Fig. 15(c). Furthermore, at the unperturbed threshold $\varepsilon_c = 0$ for $\eta = 0$ the Nusselt number takes a finite value

$$N(\varepsilon = 0) = \frac{2\eta^2}{g} \sum_{n=1}^{\infty} \frac{|\bar{c}_n|^2}{\xi_0^2(nk)^2} + \ldots\,, \tag{97}$$

which is for instance in the case of δ-correlated noise proportional to the noise amplitude D if one takes the ensemble average in Eq. (97). According to the power spectrum for correlated noise in Eq. (31), $N(\varepsilon = 0)$ will decrease with increasing values of the correlation length ℓ.

The initial slope of N is given by

$$\left.\frac{\partial N}{\partial \varepsilon}\right|_{\varepsilon_c} = \frac{1}{g}\left[1 - 4\eta^2 \sum_{n=-\infty}^{\infty}{}' \frac{|\bar{c}_n|^2}{\xi_0^4 (nk)^4} + \ldots\right], \tag{98}$$

which is in agreement with the result of the Poincaré-Lindstedt expansion for small modulation amplitudes, cf. Eq. (83), and a single realization of $M(x)$. Evaluating the ensemble average and inserting the respective power spectrum either for correlated or uncorrelated noise leads then to the respective formulas for the slope of $N(\varepsilon)$ at threshold.

5 Summary and conclusion

The effects of a spatial randomly varying contribution to the control parameter on a supercritical stationary bifurcation are strongest pronounced close to the threshold of the bifurcation, as shown by different methods in this work.

The major effects of modulations of the control parameter, the reduction of the threshold, the reduction of the initial slope $\partial N/\partial \varepsilon|_{\varepsilon_c}$ of the nonlinear function $N(\varepsilon)$ and its approach for large values of ε to the linear behavior $N(\varepsilon) \propto \varepsilon$ are all indicated by the presented perturbation calculations.

The perturbation calculation is valid in the limit of small modulation amplitudes and in section 3.1 analytical expressions are given for the mean value of the threshold reduction, the mean wave number etc.. The dependence of the respective formulas on the second moment of the noise is a considerable advantage because a determination of the threshold for each realization separately is not required before averaging. In contrast to this, with the full numerical approach the threshold has to be calculated for each realization before averaging, cf. Sec. 3.2. However, the perturbation approach fails for large values of the system length L, where the threshold reduction becomes much larger than the true one and it even diverges in the limit $L \to \infty$.

With a second semi–analytical method, the self–consistent iteration method described in section 3.3, this divergence can be avoided and the trends of the noise effects are already given in a correct manner by the lowest order of this iterative approach, even for large values of the system length. For short systems and small values of the noise amplitude, the results of the different ap-

proaches used for the threshold agree with those obtained by the perturbation calculation.

The iteration order required for the self–consistent method in order to approach the correct results, increases with the system length and the noise amplitude. So it depends on both parameters whether the computational effort is smaller for the numerical approach described in Sec. 3.2 or for the self–consistent approach in order to obtain results with reasonable precision.

For short-wavelength modulations the effects on the threshold etc. are smallest and in this limit the different approaches also provide rather similar results. The long–wavelength portions of the modulation dominate the disorder effects and with increasing values of the correlation length of the noise their effects become weaker.

Each realization of the modulation $M(x)$ gives a different threshold and the width of the distribution function obtained for an ensemble of realizations of $M(x)$ decreases for increasing values of the system length L. This suggests that in very long systems the threshold is well approximated by every realization of the underlying noise process.

The long–wavelength contributions to the noise not only affect the threshold strongly but also modify the eigensolutions at threshold that become for increasing values of the noise amplitude more and more localized, as shown in Fig. 9(a). This localization behavior also influences the Nusselt number $N(\varepsilon)$ in a characteristic manner, because slightly above threshold the nonlinear spatial structure of the solutions are quite similar to the localized eigenfunctions. These eigenstates interact with each other via the nonlinearity. Consequently, the main contributions to $N(\varepsilon)$ slightly above threshold come from the spatially extended patches of the eigensolutions and due to their spatial localization the value of the Nusselt number is smaller compared with its unperturbed value.

The localization becomes weaker for larger values of the control parameter because the spatially constant solution $\propto \varepsilon^{1/2}$ dominates. However, the spatially varying part of the nonlinear solution resembles that of the noise. This can be attributed to the decrease of the coherence length of the spatially varying portion of $A(x)$ for increasing values of D and ε, respectively, as shown in Fig. 15(d).

Spatially varying modulations that occur multiplicatively in the respective model equations leave the bifurcation sharp, but $N(\varepsilon)$ becomes rounded as a function of ε, similar as for an imperfect bifurcation. Therefore experimental curves that exhibit such a rounding may be interpreted with care as an imperfect bifurcation, because the bifurcation may still be sharp but shifted to lower values of the control parameter as a consequence of the roughness of the

container boundaries.

With our analysis of the effects of disorder within the amplitude equation for the envelope $A(x)$ of the spatially periodic real field $u(x,t) \propto A(x,t) \exp(iq_c x)+$ c.c., we have already focused on the long–wavelength modulations of the random contribution and we have restricted our approach to one spatial dimension. The noise effects in two spatial dimensions are different in several respects, as described elsewhere. The effects of a random contribution to the control parameter in a model equation with spatially periodic solutions, such as in the Swift–Hohenberg equation [44,1], are also different. In this case different kinds of resonance effects come into play, which are described elsewhere too.

References

[1] M. C. Cross, P. C. Hohenberg, Pattern formation outside of equilibrium, Rev. Mod. Phys. 65 (1993) 851.

[2] F. H. Busse, S. C. Müller (Eds.), Evolution of Spontaneous Structures in Dissipative Continuous Systems, Springer, Berlin, 1998.

[3] S. Chandrasekhar, Hydrodynamic and Hydromagnetic Stability, Oxford University Press, London, 1961.

[4] F. H. Busse, Transition to turbulence in Rayleigh–Bénard convection, in: H. L. Swinney, J. P. Gollub (Eds.), Hydrodynamic Instabilities and the Transition to Turbulence, Vol. 45 of Topic in Applied Physics, Springer, New York, 1986.

[5] R. C. DiPrima, H. L. Swinney, Instabilities and transition in flow between concentric rotating cylinders, in: H. L. Swinney, J. P. Gollub (Eds.), Hydrodynamic Instabilities and the Transition to Turbulence, Topic in Applied Physics, Springer, New York, 1981, p. 139.

[6] R. E. Kelly, D. Pal, Thermal convection with spatially periodic boundary conditions; resonant wavelength excitation, J. Fluid Mech. 86 (1978) 433.

[7] L. Kramer, E. Ben-Jacob, H. R. Brand, M. C. Cross, Wavelength selection in systems far from equilibrium, Phys. Rev. Lett. 49 (1982) 1891.

[8] D. S. Cannell, M. A. Dominguez-Lerma, G. Ahlers, Experiments on wave number selection in rotating Couette-Taylor flow, Phys. Rev. Lett. 50 (1983) 1365.

[9] M. Lowe, J. P. Gollub, T. Lubensky, Commensurate and incommensurate structures in a nonequilibrium system, Phys. Rev. Lett. 51 (1983) 786.

[10] P. Coullet, P. Huerre, Resonance and phase solutions in spatially-forced thermal convection, Physica (Nonlin. Phenomena) D 23 (1986) 27.

[11] G. Hartung, F. H. Busse, I. Rehberg, Time–dependent convection induced by broken spatial symmetries, Phys. Rev. Lett. 66 (1991) 2741.

[12] W. Zimmermann, M. Sesselberg, F. Petruccione, Effects of disorder in pattern formation, Phys. Rev. E 48 (1993) 2699.

[13] A. Ogawa, W. Zimmermann, K. Kawasaki, T. Kawakatsu, Forced periodic and quasi-periodic patterns in anisotropic systems, J. Phys. II (Paris) 6 (1996) 305.

[14] W. Zimmermann, R. Schmitz, Hopf bifurcation by frustrated drifts, Phys. Rev. E 53 (1996) R1321.

[15] R. Schmitz, W. Zimmermann, Spatially periodic modulated Rayleigh-Bénard convection, Phys. Rev. E 53 (1996) 5993.

[16] B. D. Painter, R. P. Behringer, Effects of spatial disorder on the transition to taylor–vortex flow, Europhys. Lett. 44 (1998) 599.

[17] A. D. Stroock, R. F. Ismagilov, H. A. Stone, G. M. Whitesides, Fluidic ratchet based on marangoni–bènard convection, Langmuir 19 (2003) 4358.

[18] P. Coullet, D. Walgraef, Spatial forcing of 2D wave patterns, Europhys. Lett. 10 (1989) 525.

[19] L. Howle, R. P. Behringer, J. Georgiades, Visualization of convective fluid flow in a porous medium, Nature 362 (1993) 230.

[20] W. Zimmermann, A. Ogawa, S. Kai, K. Kawasaki, T. Kawakatsu, Wavelength competition in convective systems, Europhys. Lett. 24 (1993) 217.

[21] D. M. Shattuck, R. P. Behringer, G. A. Johnson, J. G. Georgiadis, Onset and stability of convection in porous media: Visualisation by magnetic resonance imaging, Phys. Rev. Lett. 75 (1995) 1934.

[22] M. D. Shattuck, R. P. Behringer, G. A. Johnson, J. G. Georgiadis, Convection and flow in porous media, I: Visualization by magnetic resonance imaging, J. Fluid Mech. 332 (1996) 215.

[23] L. Howle, R. P. Behringer, J. G. Georgiadis, Convection and flow in porous media, II: Visualization by shadowgraph, J. Fluid Mech. 332 (1996) 245.

[24] R. Schmitz, W. Zimmermann, Orientational oscillations of stripe patterns induced by frustrated drifts, Phys. Lett. A 237 (1997) 405.

[25] W. Zimmermann, B. Painter, R. Behringer, Pattern Formation in inhomogeneous convective systems, Eur. Phys. J. B 5 (1998) 575.

[26] F. Fechner, P. Strasser, M. Eiswirth, F. W. Schneider, A. F. Münster, Spatial entrainment of pattern during the polymerization of acrylamide in the presence of the methylene blue-sulfide chemical oscillator, Chem. Phys. Lett. 313 (1999) 205.

[27] M. Dolnik, I. Berenstein, A. M. Zhabotinsky, I. R. Epstein, Spatial periodic forcing of turing structures, Phys. Rev. Lett. 87 (2001) 238301.

[28] A. Sanz-Anchelergues, A. M. Zhabotinsky, I. R. Epstein, A. P. Munuzuri, Turing pattern formation induced by spatially correlated noise, Phys. Rev. E 63 (2001) 056124.

[29] I. Berenstein, L. Yang, M. Dolnik, A. M. Zhabotinsky, I. R. Epstein, Superlattice turing structures in a photosensitive reaction-diffusion system, Phys. Rev. Lett. 91 (2003) 058302.

[30] S. Rüdiger, D. G. Miguez, A. P. Munuzuri, F. Sagués, J. Casademunt, Dynamics of turing patterns under spatiotemporal forcing, Phys. Rev. Lett. 90 (2003) 128301.

[31] I. Sendina-Nadal, A. P. Munuzuri, D. Vives, V. Perez-Munuzuri, J. Casademunt, L. Ramirez-Piscina, J. M. Sancho, F. Sagués, Wave propagation in a medium with disordered excitability, Phys. Rev. Lett. 80 (1998) 5437.

[32] O. Steinbock, P. Kettunen, K. Showalter, Anisotropy and spiral organizing centers in patterned excitable media, Science 269 (1995) 1857.

[33] M. Bär, E. Meron, C. Utzny, Pattern formation on anisotropic and heterogeneous catalytic surfaces, CHAOS 12 (2002) 204.

[34] C. Utzny, W. Zimmermann, M. Bär, Effects of spatio-temporal forcing of oscillating systems, Europhys. Lett. 57 (2002) 113.

[35] R. Neubecker, O. Jakoby, Spatial synchronization of regular optical patterns, Phys. Rev. E 76 (2003) 066221.

[36] L. Kramer, W. Pesch, Convection instabilities in nematic liquid crystals, Annu. Rev. Fluid Mech. 27 (1995) 515.

[37] A. C. Newell, J. A. Whitehead, Finite bandwidth finite amplitude convection, J. Fluid Mech. 38 (1969) 279.

[38] L. A. Segel, Distant side-walls cause slow amplitude modulation of cellular convection, J. Fluid Mech. 38 (1969) 203.

[39] C. W. Gardiner, Handbook of Stochastic Methods, Springer, Berlin, 1985.

[40] N. G. van Kampen, Stochastic Processes in Physics and Chemistry, Elsevier, Amsterdam, 2001.

[41] J. Honerkamp, Stochastic Dynamical Systems, Wiley, New York, 1993.

[42] R. C. Bourret, Stochastically Perturbed Fields, with Applications to Wave Propagation in Random Media, Nuovo Cimento Physica A 26 (1962) 1.

[43] M. Lücke, Bifurcation behavior under modulated control parameters, in: F. Moss, P. McClintock (Eds.), Noise in nonlinear dynamical systems, Vol. 2, Cambridge University Press, Cambridge, U.K., 1987, p. 100.

[44] J. B. Swift, P. C. Hohenberg, Hydrodynamic fluctuations at the convective instability, Phys. Rev. A 15 (1977) 315.